

Very Long-term Optical Variability of High Mass X-ray Binaries in the SMC

A. F. Rajoelimanana^{1,2*}, P. A. Charles^{1,3†}, and A. Udalski⁴

¹South African Astronomical Observatory, P.O. Box 9, Observatory, 7935, South Africa

²University of Cape Town, Private Bag X3, Rondebosch, 7701, South Africa

³School of Physics and Astronomy, Southampton University, Southampton SO17 1BJ

⁴Warsaw University Observatory, Aleje Ujazdowskie 4, 00-478 Warsaw, Poland

20 December 2010, accepted for publication in MNRAS

ABSTRACT

We have studied the very long-term temporal properties of the optical emission from Be X-ray binaries (BeX) in the Small Magellanic Cloud over a ~ 16 yr baseline, using light curves from the MACHO and OGLE databases. All the BeX in our sample display superorbital variations, many of them quasi-periodic on timescales of ~ 200 -3000 d. These long-term variations are believed to be related to the formation and depletion of the circumstellar disc around the Be star and we compare and contrast their behaviour with that of the LMC's prototypical BeX, A0538-66. The great majority of sources show a correlation of outburst amplitude with brightness (the opposite to that seen in A0538-66) although the amplitudes are mostly small (≤ 0.1 mag). We suggest this is an orbital inclination effect. In addition, we have also detected many of their optical orbital periodicities, visible as a series of precisely regular outbursts. Furthermore, the amplitude of these periodic outbursts can vary through the long-term superorbital cycle, and we discuss mechanisms which can produce this effect, as well as examining an apparent correlation between these periodicities. As a by-product of this variation survey we have compiled a list of all the reported SMC BeX orbital and superorbital periodicities at optical and X-ray wavelengths.

Key words:

stars: emission-line:Be - X-rays:binaries - Magellanic Clouds

1 INTRODUCTION

In high-mass X-ray binaries (HMXBs), a compact object (usually a neutron star) accretes mass from a massive early type O-B star. Conventionally, they are subdivided into two groups, the supergiant X-ray binaries (SgXRB) and Be/X-ray binaries (BeX). These massive X-ray binaries are particularly numerous in the Small Magellanic Cloud (SMC) (e.g. Coe et al. 2005).

From extrapolation of the Milky Way's population of 65 HMXBs and based on the Milky Way/SMC mass ratio being ≈ 50 , one would expect to find only one or two HMXBs in the SMC. Remarkably, 59 of these systems have now been detected, with another surprising result being that all of them are BeX systems, with only one exception, the supergiant system SMC X-1 (Coe et al. 2005; McGowan et al. 2007).

A BeX consists of a neutron star orbiting a Be star in a

wide (period \sim months) and eccentric orbit. For reasons not fully understood, Be stars rotate very rapidly, leading to outflows from the Be star that form an equatorial disc around it. If sufficiently extended, the neutron star can penetrate this equatorial disc during each periastron passage, giving rise to periodic outbursts that can be observed over a wide range of wavelengths (optical, X-ray,...) (e.g. Okazaki & Negueruela 2001). A review of basic properties of BeX can be found in Negueruela (1998) and Coe et al. (2005).

Several authors have investigated the extensive optical light curves of these sources available from the MACHO and OGLE projects in search of evidence for orbital modulations (Alcock et al. 1996; Udalski, Kubiak, & Szymanski 1997). In addition to the orbital variations usually seen as a series of periodic outbursts, these sources can show long-term superorbital modulations with timescales of hundreds of days to years. The prototype for this behaviour is the highly luminous ($\geq 10^{39}$ ergs⁻¹ at its peak) LMC BeX, A0538-66, which has a remarkably stable superorbital modulation of 420.82 days, compared to its well-established orbital period of 16.65 days (Alcock et al. 2001; McGowan & Charles 2003,

* E-mail: andry@sao.ac.za

† E-mail: pac@sao.ac.za

hereafter MC03). It was suggested by MC03 that these long-term modulations were a result of the formation and depletion of the circumstellar disc around the donor star which gives rise to the Be phenomenon. Given the known long-term variations in the Be systems, this discovery raised the question of whether such behaviour was ubiquitous, or somehow related to the presence of the X-ray source.

Consequently, in this paper, we investigate this super-orbital behaviour in much greater detail within the now substantial BeX population by exploiting the MACHO and OGLE project databases. Together these provide a 16 year baseline for LMC/SMC studies of X-ray binary counterparts. Table 1 gives the position (RA and Dec) as well as alternative name of all known SMC X-ray pulsars. We use the naming convention of Coe et al. (2005), where SXP‘x’ is the SMC X-ray Pulsar with a ‘x’ s pulse period. Table 2 details the MACHO and OGLE counterparts of these SMC X-ray pulsars, their OGLE positions (RA and Dec), all previously reported X-ray and optical orbital periods, and their X-ray luminosities.

2 OPTICAL LIGHT-CURVES FROM THE MACHO AND OGLE PROJECTS

The MACHO (MAssive Compact Halo Objects) observations were made with the 1.27 m telescope located at Mount Stromlo Observatory, Australia (Alcock et al. 1996). It provides photometry in two passbands, a red band which we refer to as \mathcal{R} -band ($\sim 6300\text{-}7600 \text{ \AA}$, a slightly longer effective wavelength than Johnson R) and a blue band we refer to as \mathcal{V} -band ($\sim 4500\text{-}6300 \text{ \AA}$, slightly shorter effective wavelength than Johnson V). The data were taken during the interval 1993 to 2000 and are available at the MACHO website¹. The data are in instrumental magnitudes.

The OGLE (Optical Gravitational Lensing Experiment) projects have used the 1.3 m Warsaw telescope at Las Campanas Observatory, Chile. Phase II of the OGLE project **ran** from January 1997 to Dec 2000 (Udalski, Kubiak, & Szymanski (1997); Zebrun et al. (2001)), and phase III from 2001 until 3 May 2009. The photometric data for the OGLE projects are taken in the I-band. OGLE II data can be downloaded from the OGLE II website². OGLE III data for optical counterparts of X-ray sources located in the fields observed regularly by the OGLE-III survey are available at the X-ray variables OGLE monitoring (XROM) website³ (Udalski 2008).

2.1 Calibrations

We used the merged OGLE II and OGLE III photometry which are relative to the final OGLE III photometry. The details of the OGLE-III calibrations which based on OGLE II photometry can be found in Udalski et al. (2008). For the MACHO data we determined what offset is needed to align them with the OGLE II data as both projects observed the SMC from 1997 to 2000, this provides substantial overlap for demonstrating their compatibility.

¹ www.macho.anu.edu.au

² ogle.astrouw.edu.pl

³ ogle.astrouw.edu.pl/ogle3/xrom/xrom.html

2.2 Temporal analysis

The combined lightcurves (~ 16 years) were then analysed using the Starlink PERIOD⁴ time-series analysis package designed to search for periodicities in unevenly sampled data. It has a variety of periodicity search options, including the Lomb-Scargle periodogram (LS periodogram, Lomb 1976; Scargle 1982), phase dispersion minimization (PDM, Stellingwerf 1978), and CLEAN algorithm (Roberts, Lehar, & Dreher 1987). The PERIOD package also has the capability to detrend and to fold any data with a given period.

2.3 Secular variability in combined datasets

In performing the temporal analyses reported here, it became clear that there were apparently significant modulations present in a few cases, but these were of low amplitude ($\sim 1\%$ peak-to-peak). Given that our data were generated from independent telescopes with different detector/filter combinations, we decided to study randomly selected field stars in order to ascertain the properties of any secular, long-term variability that this might induce. For those of our SMC fields containing BeX targets that exhibited low-amplitude modulations, we selected ~ 25 random, presumed “constant” stars for analysis in the same way as our targets.

Figure 1 summarises our results by displaying the peak L-S power observed for each random star plotted against the associated semi-amplitude (obtained by folding the data on that peak period and fitting a sine wave). Interestingly, approximately half of these random stars produced apparently significant peaks in the power spectrum (as defined by the white noise 99.9% confidence level). However, the amplitudes of these modulations are all low ($< 1\%$ peak-to-peak), and are all below the lowest amplitude modulations seen in any of our target BeX systems.

Nevertheless, where there is no independent detection of periodicities in our BeX targets (in either X-ray or optical) we have elected to report apparent detections at these low amplitudes as upper limits in table 3. This is only true in 6 cases, and has no impact on any of our subsequent results or conclusions.

It is possible that some of the highest power peaks in figure 1 are real, long-term modulations in these field early-type stars in the SMC. However, their low amplitudes will require more extensive observations and careful analysis for confirmation and follow-up. This could be an interesting research project in its own right.

3 TEMPORAL PROPERTIES OF INDIVIDUAL SOURCES

3.1 SXP0.09 (AX J0043-737)

The 87.58 ms X-ray pulsation from this source was detected by Yokogawa & Koyama (2000) during ASCA observations of the SMC on 1999 May 10-11. Optically identified as SMC-SC3 6 (Udalski 2008), this source is not how-

⁴ www.starlink.rl.ac.uk/star/docs/sun167.htx/sun167.html

Table 2. MACHO and OGLE counterparts of SMC X-ray pulsars.

Short ID	V	Spec type	Lum class	MACHO catalogue	OGLE II fields	OGLE II ID	OGLE III fields	OGLE III ID	$P_{X\text{-ray}}^\dagger$ (d)	$P_{opt}^{*\dagger}$ (d)	Log L_X (max) (erg.s^{-1})
SXP0.09	16.9				SMC-SC3	6	SMC128.4	118			34.9 [0.7-10 keV]
SXP0.92	16.1	B0.5-B2	IV-V	212.15676.64	SMC-SC3	197970	SMC125.3	19461		51 ^[1] [R]	
SXP2.37	16.3	O9.5	III-V				SMC107.5	25			38.6 [2-25 keV]
SXP2.76	14.0	B1-B1.5	II-III				SMC109.2	5		82.1 ^[2] [O]	37.7 [0.1-2 keV]
SXP3.34	15.6	B1-B2	III-V	206.16890.17	SMC-SC10	102553					35.1 [0.1-2 keV]
SXP4.78	15.8	B0-B1	V	207.16146.9					34.1	23.9 ^[3] [M]	37.8 [3-10 keV]
SXP6.85	14.5	O9.5-B0	IV-V	206.16768.5	SMC-SC9	146936			112	114 ^[4] [OM]	37.5 [2-30 keV]
SXP7.78	14.9	B1-B1.5	IV-V	208.16088.4			SMC101.3	33277	44.9	44.8 ^[5] [OM]	37.7 [2-10 keV]
SXP7.92	13.9	O9		207.16714.4	SMC-SC9	114259	SMC110.5	5		36.8 ^[14] [O]	36.8 [0.3-10 keV]
SXP8.9	14.8	O9.5-B0	IV-V	208.16087.9	SMC-SC6	85614	SMC101.3	4737	28.4	33.4 ^[6] [OM]	36.1 [0.1-2 keV]
SXP9.13	16.5	B1-B3	IV-V	212.15906.2446	SMC-SC5	111490	SMC100.7	63223	77.2	40.1 ^[8] [O]	35.6 [0.7-10 keV]
SXP15.3	14.6	O9.5-B0	III-V	212.16075.13	SMC-SC6	99923	SMC100.1	48026	28	75.1 ^[8] [OM]	37.1 [0.1-2 keV]
SXP18.3	15.6	B0-B2	V	208.15911.13	SMC-SC5	65500	SMC101.8	19552	17.7	17.7 ^[15] [O]	37.5 [0.2-10 keV]
SXP22.1	14.1	O9.5-B0	III-V				SMC116.1	3322			38.0 [0.1-2 keV]
SXP25.5	15.2			212.15849.52	SMC-SC4	171264	SMC100.7	54315			35.3 [0.2-10 keV]
SXP31.0	15.5	O9.5-B1	V				SMC116.6	33		90.4 ^[2] [O]	38.3 [0.1-2 keV]
SXP34.1	16.7	B2-B3	IV-V				SMC108.7	24657			35.0 [0.3-10 keV]
SXP46.6	14.7	O9.5-B1	IV-V				SMC108.8	30	137	137 ^[9] [O]	36.8 [0.1-2 keV]
SXP59	15.2	O9	V	207.16259.23	SMC-SC7	70829	SMC105.5	35420	122	60.2 ^[10] [OM]	37.6 [2-10 keV]
SXP65	15.6	B1-B1.5	II-III						110		35.8 [0.2-10 keV]
SXP74.7	16.9	B3	V	208.15911.93	SMC-SC5	65517	SMC100.5	55158	61.6	33.4 ^[11] [O]	36.7 [0.7-10 keV]
SXP82.4	15.0	B1-B3	III-V	208.16085.24	SMC-SC6	77228	SMC101.2	12997	362		36.5 [0.3-10 keV]
SXP91.1	15.0	B0.5	III-V	208.16034.5			SMC102.1	32	117	88.2 ^[7] [M]	37.4 [0.1-2 keV]
SXP101	15.6	B3-B5	Ib-II	211.16415.11			SMC106.7	15343	25.2	21.9 ^[12] [OM]	36.0 [0.7-10 keV]
SXP138	16.1	B1-B2	IV-V	207.16202.50			SMC101.3	38781	103	125 ^[8] [M]	35.0 [0.3-10 keV]
SXP140	15.8	B1	V	207.16374.21			SMC108.8	35838		197 ^[6] [M]	34.6 [0.1-2 keV]
SXP152	15.6	B1-B2.5	III-V				SMC108.3	36			35.6 [0.1-2 keV]
SXP169	15.5	B0-B1	III-V				SMC102.2	13410	68.5	67.6 ^[2] [O]	37.3 [0.1-2 keV]
SXP172	14.4	O9.5-B0	V	212.16077.13	SMC-SC6	22749	SMC100.2	44100	70	69.9 ^[6] [O]	36.0 [0.2-10 keV]
SXP202A	14.8	B0-B1	V	207.16545.12	SMC-SC8	151891	SMC108.1	4929	91		35.5 [0.2-10 keV]
SXP202B	15.6	B0-5	III	207.16541.15	SMC-SC8	139407	SMC105.3	29894			36.6 [0.2-10 keV]
SXP264	15.8	B1-B1.5	V	212.15792.77	SMC-SC4	116979	SMC100.7	45007		49.1 ^[10] [O]	36.2 [0.2-10 keV]
SXP280	15.6	B0-B2	III-V				SMC108.3	16091	64.8	127 ^[2] [O]	36.2 [0.1-2 keV]
SXP293	14.9	B2-B3	V	207.16486.9	SMC-SC8	94537	SMC105.4	22335	151	59.7 ^[7] [OM]	35.6 [0.2-10 keV]
SXP304	15.7	B0-B2	III-V	206.16663.16	SMC-SC9	47428	SMC108.3	12190		520 ^[6] [M]	36.1 [0.1-2 keV]
SXP323	15.4	B0-B0.5	V	212.16019.30	SMC-SC5	180026	SMC100.2	48	116		35.4 [0.2-10 keV]
SXP327	16.3			207.16147.60			SMC101.4	25097		45.9 ^[16] [O]	35.5 [0.2-10 keV]
SXP348	14.7	B0.5	IV-V	206.16776.17	SMC-SC9	173121	SMC108.8	33		93.9 ^[6] [O]	36.0 [0.1-2 keV]
SXP455	15.4	B0.5-B2	IV-V	206.16662.14	SMC-SC9	89374	SMC108.2	34801		74.7 ^[7] [OM]	35.8 [0.7-10 keV]
SXP504	14.9	B1	III-V	207.16254.16	SMC-SC7	47103	SMC105.7	36877	265	273 ^[10] [O]	35.7 [0.3-10 keV]
SXP564	15.9	B0-B2	IV-V	207.16432.1575	SMC-SC8	49531	SMC108.1	19293	151	95.3 ^[7] [M]	34.8 [0.3-10 keV]
SXP645	14.6	B0-B0.5	III-V	207.16315.28	SMC-SC7	137527	SMC105.5	35415			35.6 [0.2-10 keV]
SXP701	15.8	O9.5	V	207.16313.35	SMC-SC7	129062	SMC105.6	36015		412 ^[10] [M]	35.6 [0.2-10 keV]
SXP726	15.6	B0.5-B3			SMC-SC10	137851	SMC113.3	10946			34.8 [0.1-2 keV]
SXP755	14.9	O9.5-B0	III-V	212.15960.12	SMC-SC5	90506	SMC100.8	22903	389	394 ^[7] [M]	35.9 [0.2-10 keV]
SXP893	16.3				SMC-SC5	111500	SMC100.7	63151			34.5 [2-10 keV]
SXP967	14.6	B0-0.5	III-V				SMC114.7	39			35.9 [0.2-10 keV]
SXP1323	14.6	B0	III-V		SMC-SC10	37138	SMC113.6	27699		26.1 ^[2] [O]	36.8 [0.2-10 keV]

[1]: Kaspi et al. (1993) ; [2]: Schmidtke & Cowley (2006); [3]: Coe et al. (2005) ; [4]: McGowan et al. (2008) ; [5]: Cowley & Schmidtke (2004) ; [6]: Schmidtke, Cowley, & Udalski (2006) ; [7]: Schmidtke et al. (2004) ; [8]: Edge (2005a) ; [9]: McGowan et al. (2008) ; [10]: Schmidtke & Cowley (2005b) ; [11]: Schmidtke & Cowley (2007b) ; [12]: McGowan et al. (2007) ; [13]: Edge et al. (2005b); [14]: Coe et al. (2009); [15]: Schurch et al. (2009); [16]: Udalski & Coe (2008)

[†] X-ray orbital period from Galache et al. (2008) paper.

[‡] Previously reported optical orbital period.

* Source of P_{opt} : M for MACHO project, O for OGLE, OM for both of the data, and R for radio.

ever present in the catalogue of emission-line stars and PNe (Meyssonnier & Azzopardi 1993, hereafter MA93).

Figure 2a shows the combined OGLE II and OGLE III lightcurve of SXP0.09 (MACHO data is not available) which is very steady, to within ± 0.05 mag. Its orbital period has not yet been reported, but both the LS periodogram and PDM revealed a strong peak well above the 99.9 % confi-

dence level relative to both white and red noise ⁵ at a period of 247 ± 5 d (Figure 2c). We did not find any significant shorter period in the periodogram (Figure 2b).

⁵ Red noise is calculated using REDFIT (Schulz 2002) (www.ncdc.noaa.gov/paleo/softlib/redfit/redfit.html)

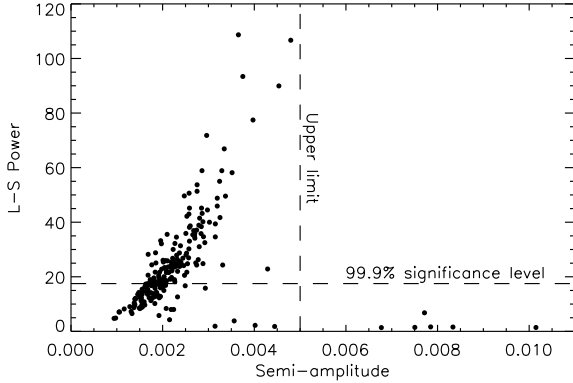


Figure 1. The peak L-S power observed for 221 random stars selected from fields where low amplitude modulations had been detected in our BeX target. These are plotted against the associated semi-amplitude and allow us to set a limit of 5 mmag for any real modulation. The 99.9% confidence level for significant periods in terms of the L-S power are based on white noise calculations.

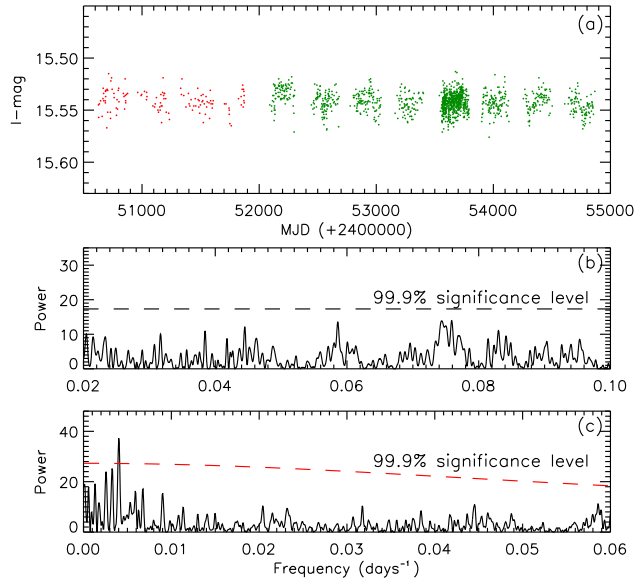


Figure 2. SXP0.09. (a): OGLE II (red) and OGLE III (black) light curves. (b) and (c): Lomb-Scargle power spectrum of the OGLE data with a significant peak at $P=247$ d, the red dashed line represents the 99.9% confidence level relative to the “red” noise.

3.2 SXP0.92 (PSR J0045-7319)

SXP0.92 was first discovered by Ables et al. (1987) as a 0.926499 s radio pulsar. Bell (1994) identified its optical companion as a 16th magnitude, 11 M_{\odot} , B1 main-sequence star. The orbital period (51 d) of PSR J0045-7319 was found by Kaspi et al. (1993) through the Doppler modulation of the pulse period.

Our combined light curve of SXP0.92 (Figure 3a) reveals no optical signature of the 51 d periodicity, but it does clearly display an almost sinusoidal ~ 2600 d superorbital modulation. This appears as a strong peak in the LS pe-

Table 1. List of all known SMC X-ray pulsars.

Short ID	RA (2000)	Dec (2000)	Alternative [†] Name
SXP0.09	00:42:35.4	-73:40:34	AX J0043-737
SXP0.72	01:17:05.5	-73:26:32	2U 0115-737, SMC X-1
SXP0.92	00:45:35.0	-73:19:02	PSR J0045-7319
SXP2.16	01:19:51.0	-73:11:48	XTE J0119-731
SXP2.37	00:54:36.2	-73:40:35	H 0053-739, SMCX-2
SXP2.76	00:59:11.3	-71:38:45	RX J0059.2-7138
SXP3.34	01:05:09.7	-72:11:46	AX J0105-722, [MA93] 1506
SXP4.78	00:52:06.6	-72:20:44	XTE J0052-723, [MA93] 537
SXP6.85	01:03:24.0	-72:43:00	XTE J0103-728
SXP7.78	00:52:07.7	-72:25:50	2S 0050-727, [MA93] 531
SXP7.92	01:01:56.0	-72:32:36	AZV285
SXP8.02	01 00 43.1	-72 11 33	PSR J0100-7211
SXP8.9	00:51:53.0	-72:31:45	RX J0051.8-7231,[MA93]506
SXP9.13	00:49:13.8	-73:11:36	RX J0049.2-7311
SXP11.5	01 04 41.4	-72 54 04	IGR J01054-7253
SXP15.3	00:52:13.9	-73:19:13	RX J0052.1-7319,[MA93]552
SXP16.6	00:50:00.0	-73:16:00	XTE J0050-732#1
SXP18.3	00:49:11.4	-72:49:37	XMMJU004911.4-724939
SXP22.1	01:17:41.4	-73:30:49	RX J0117.6-7330
SXP25.5	00:48:14.1	-73:10:03	XMMU J004814.1-731003
SXP31.0	01:11:08.4	-73:16:46	XTE J0111.2-7317
SXP34.0	00:55:27.7	-72:10:59	CXOU J005527.9-721058
SXP46.4	00:51:00.0	-73:18:00	XTE SMC46
SXP46.6	00:53:55.0	-72:26:47	1WGA J0053.8-7226
SXP51	00:50:00.0	-73:16:00	XTE J0050-732#2
SXP59	00:54:56.1	-72:26:27	XTE J0055-724, [MA93] 810
SXP65.8	01:07:12.6	-72:35:33	CXOU J010712.6-723533
SXP74.7	00:49:02.5	-72:50:52	AX J0049-729
SXP82.4	00:52:09.1	-72:38:03	XTE J0052-725
SXP89.0	00:53:54.0	-72:26:42	XTE POSITION A
SXP91.1	00:50:55.8	-72:13:55	RX J0051.3-7216, [MA93] 413
SXP95	00:53:24.0	-72:49:18	XTE SMC95
SXP101	00:57:26.8	-73:25:02	AX J0057.4-7325
SXP138	00:53:23.8	-72:27:15	CXOUJ005323.8-722715
SXP140	00:56:05.2	-72:22:00	XMMUJ005605.2-722200
SXP144			XTE SMC144s
SXP152	00:57:50.3	-72:07:56	CXOUJ005750.3-720756
SXP164	01:05:00.0	-72:06:21	XTE POSITION B
SXP169	00:52:59.2	-71:57:58	RX J0052.9-7158, [MA93] 623
SXP172	00:51:52.2	-73:10:33	RX J0051.9-7311, [MA93] 504
SXP202A	00:59:21.0	-72:23:16	1XMMU J005921.0-722317
SXP202B	00:59:28.6	-72:37:03	XMMUJ005929.0-723703
SXP264	00:47:23.4	-73:12:27	RX J0047.3-7312, [MA93] 172
SXP280	00:57:48.4	-72:02:42	RX J0057.8-7202, [MA93]1036
SXP293	00:58:11.7	-72:30:50	RX J0058.2-7231
SXP304	01:01:01.1	-72:06:57	RX J0101.0-7206, [MA93]1240
SXP323	00:50:44.7	-73:16:05	RX J0050.7-7316, [MA93]387
SXP327	00:52:52.2	-72:17:14	XMMU J005252.1-721714.7
SXP348	01:03:13.9	-72:09:14	AX J0103-722, [MA93] 1367
SXP455	01:01:20.5	-72:11:18	RX J0101.3-7211, [MA93]1257
SXP504	00:54:55.8	-72:45:10	AX J0054.8-7244, [MA93]809
SXP564	00:57:36.2	-72:19:34	CXOUJ005736.2-721934
SXP645	00:55:35.1	-72:29:06	XMMU J005535.2-722906
SXP701	00:55:18.4	-72:38:51	XMMU J005517.9-723853
SXP726	01:05:55.3	-72:03:47	RX J0105.9-7203, [MA93]1557
SXP755	00:49:42.0	-73:23:15	RX J0049.7-7323, [MA93]315
SXP893	00:49:29.8	-73:10:58	
SXP967	01:02:06.7	-71:41:15	CXOU J010206.6-714115
SXP1323	01:03:37.5	-72:01:33	RX J0103.6-7201, [MA93]1393

[†] [MA93] is related to the catalogue of emission-line stars and PNe by Meyssonnier & Azzopardi (1993).

riodogram at a frequency corresponding to 2654 ± 298 d (Figure 3c). The folded light curve on this period is shown in Figure 3d. Whilst this periodicity is very close to half the total observing time, the modulation is in fact clearly visible in the raw light curve (Figure 3a).

We did not find any significant peak at the previously reported 51 d period, but the data folded on this pe-

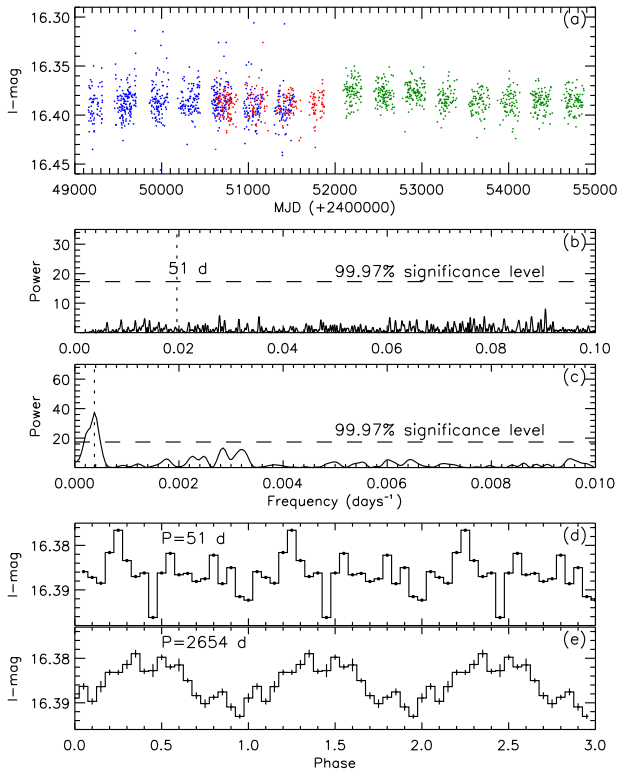


Figure 3. SXP0.92. (a): MACHO \mathcal{R} -band (blue), OGLE II (red) and OGLE III (green) light curves. (b) and (c): power spectrum of the combined data showing the peak at $P=2654$ d. (d) and (e): Combined data light curve folded on the 51 d presumed orbital period and the superorbital period of 2654 days.

riod shows a low amplitude (≤ 0.01 mag) modulation (Figure 3d).

3.3 SXP2.37 (SMC X-2)

SMC X-2 is a long-established X-ray source detected in the SMC by SAS-3 (Li, Jernigan, & Clark 1977). The optical counterpart of SMC X-2 was identified by Pesch, Sanduleak, & Philip (1977) as a 14th magnitude OB star, and this identification was supported by spectroscopic observations (Allen 1977).

Schurch, Udalski, & Coe (2008) found a variation in the OGLEIII data of SXP2.37 with a period of 18.62 ± 0.02 d, and proposed that it is the orbital period. However, Schmidtke, Cowley, & Udalski (2009) have suggested that this modulation is not orbital, but is instead the beat period between two non-radial pulsations ($P=0.8592$ d and 0.9008 d) of the primary star. We note that our OGLE III data has only one data point per night (only 3 nights have two). The OGLE III light curve of SXP2.37 clearly shows the 18.6 d variation (Figure 4a). We have detrended the OGLE III data and found peaks at 18.58 ± 0.003 d, and its harmonics at 9.3 and 6.2 d (see Figure 4c), which is similar to those reported by Schurch, Udalski, & Coe (2008). The light curve folded on the 18.58 d period shows interesting evolution from apparent maxima to dips in each cycle (Figure 4d and e). This will be discussed further later.

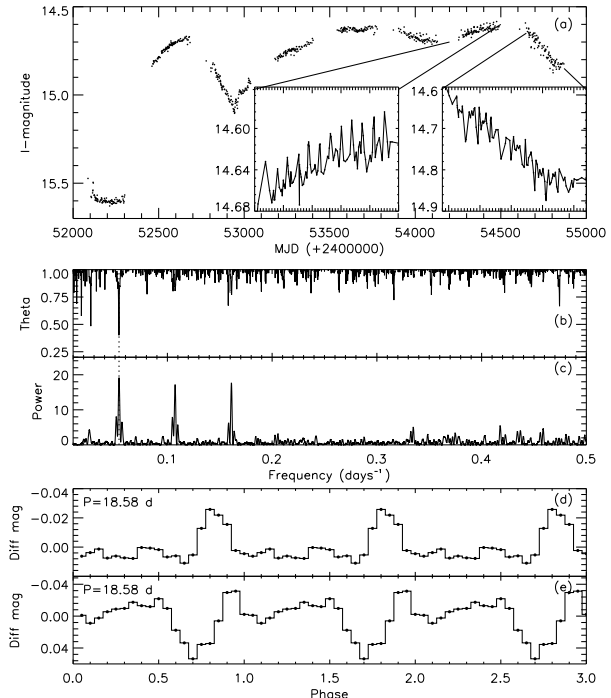


Figure 4. SXP2.37 : (a): OGLE III light curve with (inset) the blow-up of a section of data that displays a low amplitude modulation (outbursts and dips) at 18.58 d. (b) and (c): Periodogram (PDM and LS) of the OGLE III data with a highest peak at $P=18.58$ d, and its harmonics at 9.3 d and 6.2 d. (d) and (e): Light curve showing outbursts (MJD 53800- 54500) and dips (MJD 54600- 55000), respectively, folded on the presumed 18.58 d orbital period.

3.4 SXP2.76 (RX J0059.2-7138)

The 2.76 s pulsation from RX J0059.2-7138 was detected with ROSAT (Hughes 1994). Schmidtke & Cowley (2006) found the orbital period of SXP2.76 which is clearly seen as repeated, low-amplitude outbursts every 82.1 days.

The source lies outside MACHO and OGLE II fields, but the OGLE III light curve for this X-ray pulsar (Figure 5a) shows an exceptionally clear sinusoidal variation of large (~ 0.2 mag) amplitude with a period of about 2800 d, which is comparable to the duration of the dataset. The first half of the detrended data (before MJD 53500) shows a very regular set of outbursts on the orbital period $P_{\text{orb}} = 82 \pm 0.07$ d (Figure 5b). In the second half, the amplitude of these outbursts is very low, and they completely disappear during global minimum. The power spectrum of the detrended second part of the OGLE III data does not show any significant peak (Figure 5c).

3.5 SXP3.34 (AX J0105-722)

Coe et al. (2005) identified the optical counterpart of AX J0105-722 as MA[93]1506 and found a period of 11.09 d in the MACHO data which they proposed to be the orbital period. However, Schmidtke & Cowley (2005a) again reported the presence of non-radial pulsations in the same MACHO

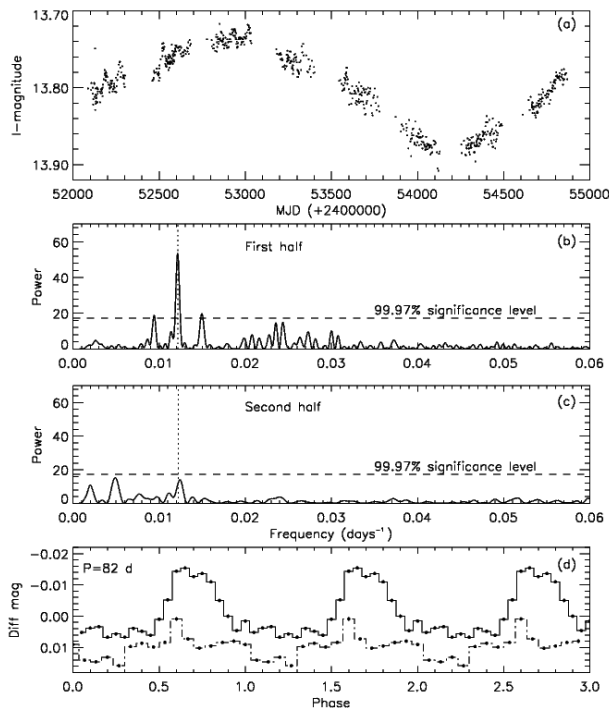


Figure 5. SXP2.76: (a): OGLE III light curve. (b) and (c): power spectrum of the 1st (before MDJ 53500) and 2nd half of the detrended OGLE III data. (d): First (solid) and second (dashed) half of the OGLE III light curve folded on the period of 82 d.

data, the period being 1.099 d. They also suggested that the 11.09 d signal is an alias of this shorter period.

The combined MACHO and OGLE II light curve of SXP3.34 is presented in Figure 6a and is very stable to within ± 0.05 mag, although a several hundred day modulation is discernible. Our power spectrum shows a significant peak at 11.07 ± 0.01 d (Figure 6b). The light curve folded on the 11.07 d period is shown in Figure 6e. The LS periodogram of the combined light curve shows a significant peak at 99% confidence level with a much longer, but low amplitude super-orbital period of 495 ± 2 d (Figure 6c).

3.6 SXP6.85 (XTE J0103-728)

X-ray pulsations at 6.85 s from XTE J0103-728 were first detected by Corbet et al. (2003a). Subsequently, an accurate position was determined with XMM-Newton by Haberl, Pietsch, & Kahabka (2007) during an outburst in 2006 October, from which they identified the optical counterpart as a 14th magnitude Be star. Schmidtke & Cowley (2007a) have analyzed its lightcurve from MACHO observations and suggested an orbital period of 24.82 d. However, from the combined MACHO and OGLE datasets McGowan et al. (2007) found an optical period of 114 d which is similar to the X-ray period of 112.5 d reported by Galache et al. (2008) and is presumed to be orbital in origin.

We have detrended the complete datasets from MACHO, OGLE II and OGLE III, and found a significant peak at 110 ± 0.2 d (Figure 7c), which is very similar to the previously reported periods. The folded light curve on this period

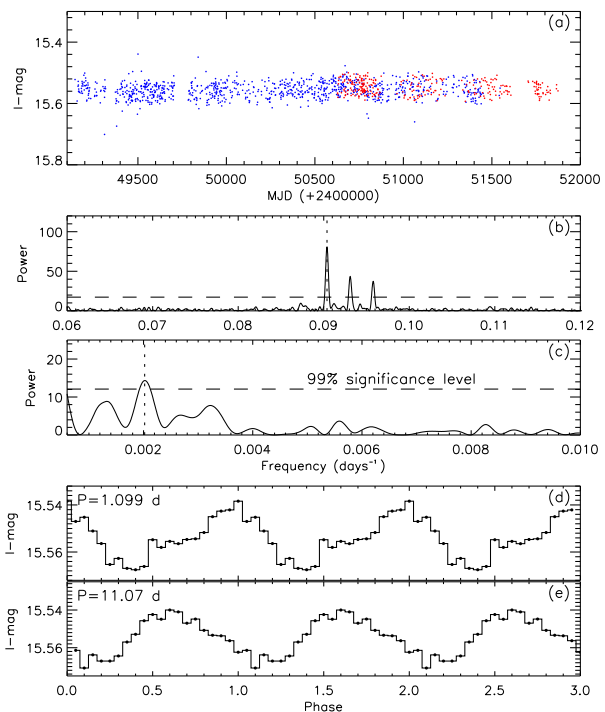


Figure 6. SXP3.34: (a): MACHO \mathcal{R} -band (blue) and OGLE II (red) light curves. (b) and (c) : Power spectrum of the combined light curve showing peaks at 11.07 d and 495 d. (d) and (e): Light curve folded on the period of 1.099 d, 11.07 d respectively.

shows a transient-like profile typical of BeX systems (Figure 7e).

The MACHO and OGLE light curves are presented in Figure 7a, and reveal a long-term variation of very large amplitude (≥ 0.5 mag). The power spectrum of the combined MACHO and OGLE light curves shows a large peak at 621 ± 4 d which is consistent with the ‘recurrence time’ mentioned by Schmidtke & Cowley (2007a).

The colour variation of SXP6.85 is also plotted, and the source is brighter when it is redder (Figure 7b). This is the opposite to that seen in A0538-66 where the source is bluer when it is brighter and strong outbursts occur only during optical minimum (Alcock et al. 2001). It is interesting to note that the color variation continues to increase until ~ 100 days after the maximum brightness of the source, i.e., there is an offset (or lag) between the maximum of colour and brightness variations.

McGowan et al. (2007) have not found any correlation between X-ray and optical activity for this source and suggest that it could be a low eccentricity system.

3.7 SXP7.78 (2S 0050-727)

The optical counterpart of SXP7.78 is MA[93]531 or MACHO 208.16088.4 (Coe et al. 2005). From X-ray observations with RXTE, Galache et al. (2008) found a series of outbursts with a period of 44.92 ± 0.06 d which is consistent with the presumed orbital period of 44.6 d found in the MACHO \mathcal{R} lightcurve (Coe et al. 2005).

The OGLE III lightcurve in Figure 8b shows clearly the regular orbital outbursts, as is also reflected in the power

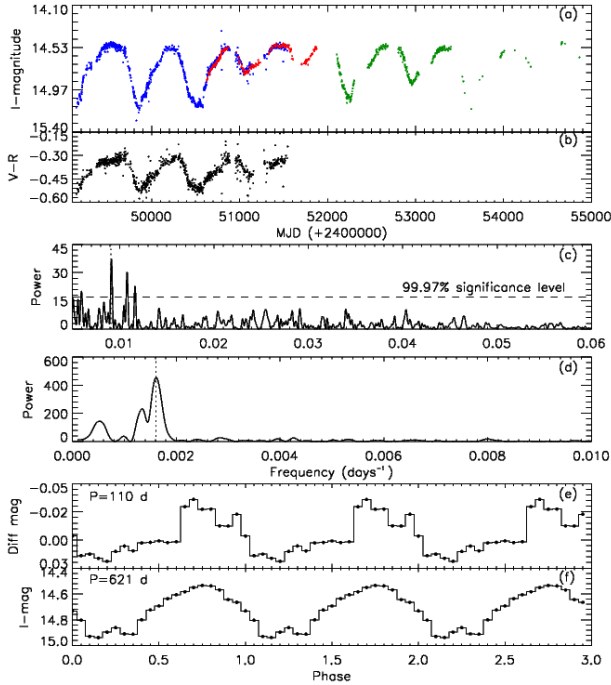


Figure 7. SXP6.85: (a): MACHO and OGLE light curves. (b) MACHO colour variation ($V - R$). (c) and (d): Power spectrum of the detrended and combined light curves showing significant peaks at 110 d and 621 d respectively. (e) and (f): Light curve folded on the 110 d and 621 d.

spectrum of the detrended data at a period of 44.92 ± 0.2 d (Figure 8c). It is also clear that the amplitude of the outbursts vary with the source brightness.

The combined MACHO and OGLE III light curves of Figure 8a show substantial long-term variability, which is responsible for the LS power spectra peaks at 1116 ± 56 d, and 2029 ± 186 d. The peak at 0.002739 d^{-1} ($P=365$ d) is due to the annual sampling of the data.

SXP7.78 is one of the BeX systems which shows clear optical periodic outbursts even when the source is at optical minimum in the superorbital cycle (see Figure 8b). Furthermore, the strength of its outbursts appears to vary with its optical brightness, being very strong at optical maximum, but always present throughout the 2029 d cyclic variation.

3.8 SXP7.92 (AZV 285)

The pulse period of 7.92 s of this source was discovered recently by Corbet et al. (2008) using RXTE/PCA. Its possible optical counterpart is discussed in Coe et al. (2009), who identified it as AzV285 with an orbital period of 36.8 d.

The power spectrum of the long-term combined light curve reveals strong low-frequency power, with a peak at 397 ± 2 d (Figure 9d) and the detrended light curves show a peak at 36.4 ± 0.02 d (Figure 9c), very similar to the presumed orbital period. The folded light curves on these periods are presented in Figure 9e and 9f, where the long-term one has a clear asymmetric profile.

The light curve of SXP7.92 exhibits large (~ 1 mag) variations and becomes redder when it is brighter (suggesting

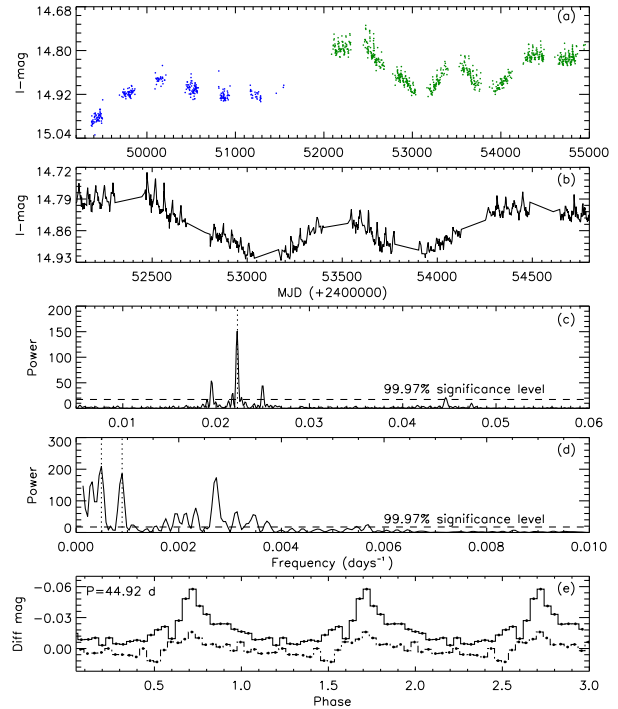


Figure 8. SXP7.78. (a): MACHO R -band (blue) and OGLE III (green) light curves. (b): Blow-up of the OGLE III light curve. (c) and (d): Power spectrum of the detrended and combined data with maximum peaks at 44.92d, 1116 d and 2029 d (the peak at 0.002739 d^{-1} is due to the annual sampling). (e): detrended light curve folded on the orbital period of 44.92 d when optically bright (solid line) and faint (dashed line).

a low inclination system), and the orbital modulation is always present. But, as seen in the OGLE III light curve (Figure 10), when the Be star is close to maximum ($I \sim 13.7$), the strength of the normal periodic modulation becomes very weak. Optically at maximum, SXP7.92 is the brightest BeX system in the SMC.

3.9 SXP8.88 (RX J0051.8-7231)

This source was discovered to be an X-ray pulsar by Israel et al. (1997). Its optical counterpart was proposed by Haberl & Pietsch (2004) to be MA[93]506. Schmidtke, Cowley, & Udalski (2006) found a weak period of 33.4 d in the early OGLE II data which they suggested as the orbital period. From RXTE observations of the SMC, Corbet et al. (2004a) suggested an X-ray orbital period of 28.47 d.

Given the large amplitude long-term variation present in the combined MACHO and OGLE lightcurves of SXP8.88 (Figure 11a), it is not surprising that the power spectrum has significant low-frequency power with a peak at 1786 ± 32 d (Figure 11d).

We have only selected and detrended the data during the bright phase (MJD 51000-52000 and MJD 52400-53400). The power spectrum of our detrended OGLE light curve shows a significant peak at a period of 28.51 ± 0.01 d which is very close to the X-ray period reported by Corbet et al. (2004a) (Figure 11c). The folded light curve on this 28.51

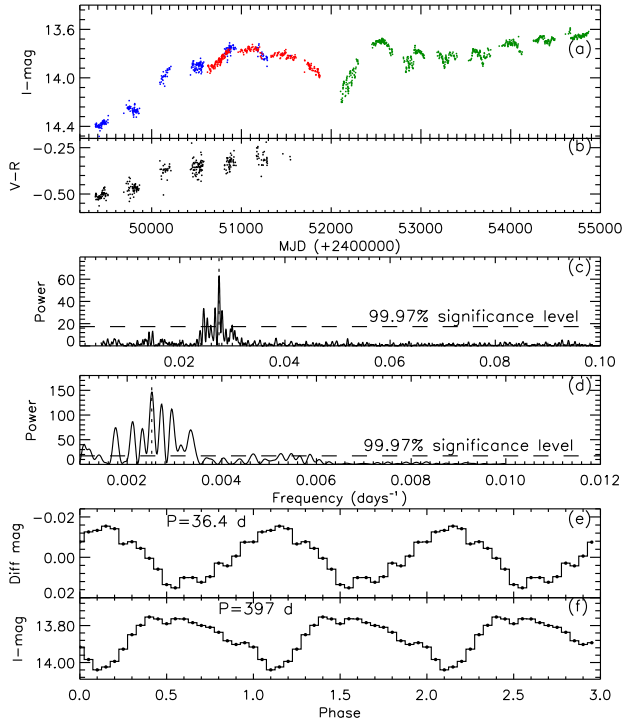


Figure 9. SXP7.92. (a): MACHO \mathcal{R} -band (blue), OGLE II (red) and OGLE III (green) light curves. (b): MACHO colour variation ($V-R$). (c) and (d): Power spectrum of the combined data showing peaks at $P=36.4$ d and $P=397$ d. (e) and (f): Folded light curves on the periods of 36.4 d and 397 d respectively.

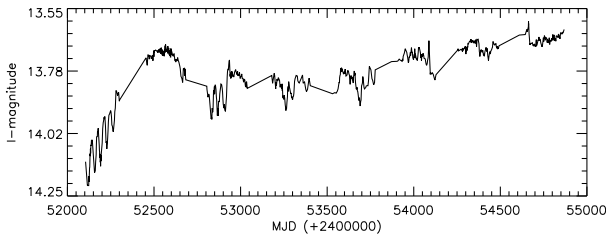


Figure 10. SXP7.92. Blow-up of the OGLE III light curve.

d period is shown in Figure 11e, however, the amplitude is very weak.

3.10 SXP9.13 (AX J0049-732)

This source was found to be a 9.1321 s X-ray pulsar by Imanishi, Yokogawa, & Koyama (1998). Schmidtke et al. (2004) proposed RX J0049.5-7310 as a ROSAT counterpart of this ASCA pulsar. However, Coe et al. (2005) pointed out that RX J0049.5-7310 lies well outside the revised X-ray error circle presented in Ueno et al. (2001) and proposed RX J0049.2-7311 to be the more likely ROSAT counterpart, and identified its optical counterpart. A period of 40.17 d was reported by Edge (2005a), however Galache et al. (2008) suggested an X-ray orbital period of 77.2 ± 0.3 d.

We detrended the OGLE II and OGLE III data by subtracting a linear fit to the long-term trends. The periodograms revealed a peak at 80.1 ± 0.06 d in both PDM and

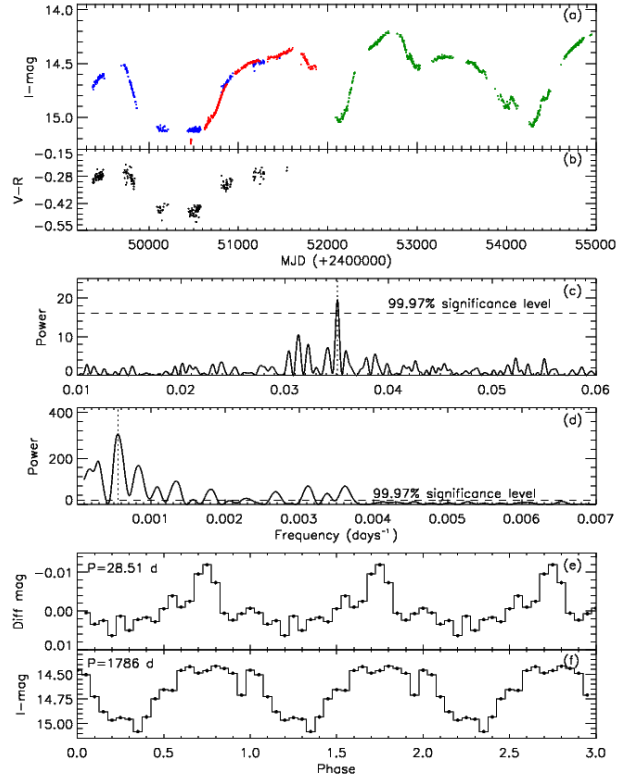


Figure 11. SXP8.88. (a): MACHO \mathcal{R} -band (blue), OGLE II (red) and OGLE III (green) light curves. (b): MACHO colour variation ($V-R$). (c) and (d): power spectrum of the detrended and combined data with highest peaks at $P=28.51$ d and $P=1786$ d. (e) and (f): Light curve folded on periods of 28.51 d and 1786 d respectively.

L-S periodograms, plus its harmonics at 20, 26.6 and 40 d (figure 12b and 12c). This period is very similar to the X-ray orbital period found by Galache et al. (2008) and twice the optical period reported by Edge (2005a). The folded light curve on the period of 80.1 d is shown in Figure 12e. The shape of the light curve is unusual with a dip of low amplitude.

The power spectrum of the combined long-term light curves has a strong peak with a superorbital period of 1886 ± 35 d (Figure 12d). The folded light curve on this long period is shown in Figure 12f.

3.11 SXP15.3 (RX J0052.1-7319)

The 15.3 s pulsations from RX J0052.1-7319 were discovered by Lamb et al. (1999). Subsequently, Israel et al. (1999) proposed its optical counterpart to be a B-type star, which was confirmed spectroscopically by Covino et al. (2001).

The combined MACHO and OGLE light curves (Figure 13d) display substantial, long-term, quasi-periodic variations of 1515 ± 23 d, and the light curve folded on this superorbital period is shown in Figure 13f. The power spectrum of the detrended OGLE II and OGLE III light curves also show a peak at 74.5 ± 0.05 d (Figure 13c) which is consistent with the orbital period of 75.1 d found by Edge (2005a). Figure 13e shows the detrended light curve folded on this

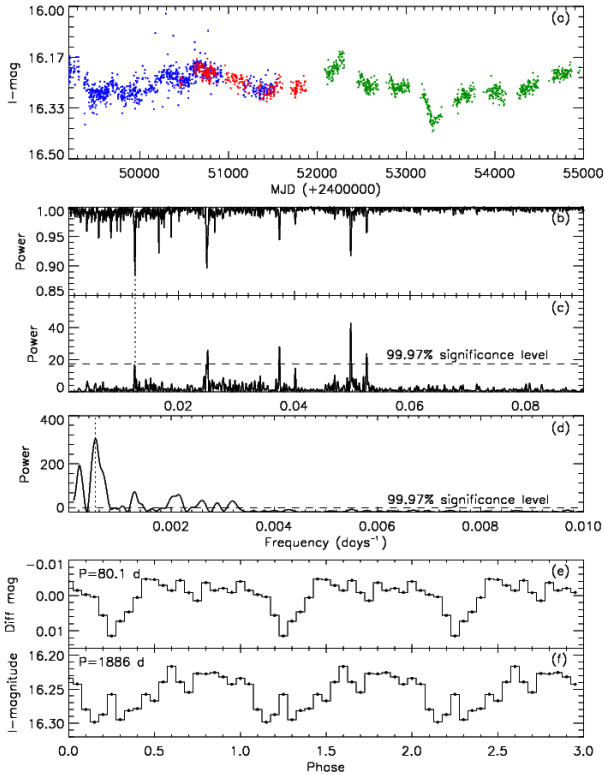


Figure 12. SXP9.13. (a): MACHO \mathcal{R} -band (blue), OGLE II (red) and OGLE III (green) light curves. (b) and (c): Power spectra (PDM and L-S) of the detrended light curve. (d): Power spectrum of the combined light curve. (e) and (f): Light curve folded on periods of 80.1 d and 1886 d respectively.

period. The 74.5 d modulation is present throughout the 1515 d cycle.

3.12 SXP18.3 (XMMJU004911.4-724939)

This X-ray source was discovered to be an X-ray pulsar by Corbet et al. (2003b) with a period of 18.37 ± 0.01 s. The XMM-Newton position (Eger & Haberl 2008) allowed its optical counterpart to be identified as a $V=16$ star (Zaritsky et al. 2002). A presumed orbital period of 17.79 d was found using both optical (Udalski & Coe 2008; Schurch et al. 2009), and X-ray observations (Galache et al. 2008). The temporal analysis finds no significant long-term periodicities in the combined light curves, although there are extreme excursions (≥ 1 mag) on timescales of ~ 2000 d (Figure 14a). In Figure 14b, it is clear that the source becomes redder when it brightens.

We have detrended the MACHO and OGLE datasets and examined their temporal properties in sections with surprising results. The light curves from the MACHO, OGLE II, and the first year of OGLE III data show a clear variation of 28.5 ± 0.01 d, which appears as a significant peak in its power spectrum (Figure 14c and 14d). The folded light curve on this period (Figure 14f) shows a clear sinusoidal variation. However, for the OGLE III data (from MDJ 53000), its power spectrum shows a significant peak at a period of 17.9 ± 0.01 d (Figure 14e), which is very similar to the re-

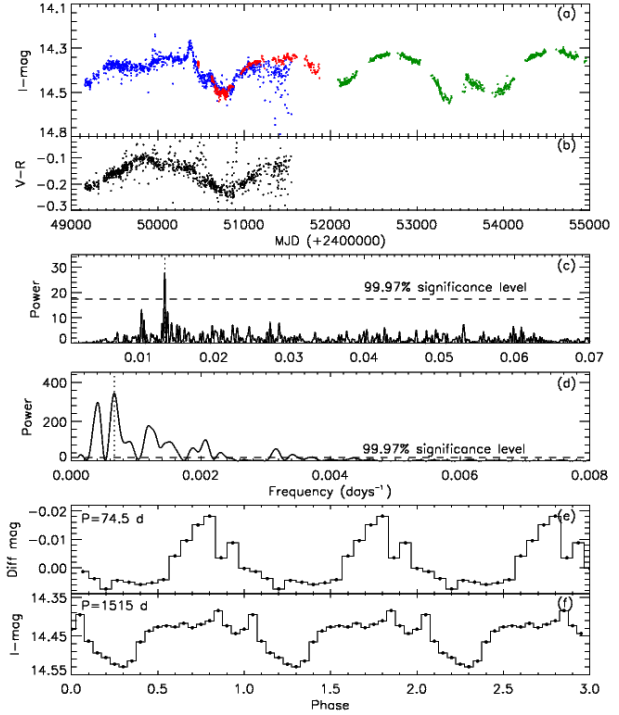


Figure 13. SXP15.3. (a) MACHO \mathcal{R} -band (blue), OGLE II (red) and OGLE III (green) light curves. (b) MACHO colour variation ($V - \mathcal{R}$). (c) and (d): Power spectrum of the detrended and combined light curve showing peaks at $P=74.5$ d and $P=1515$ d respectively. (e) and (f): Light curve folded on periods of 74.5 d and 1515 d respectively.

ported X-ray 17.73 d period by Galache et al. (2008). The folded light curve on this period is shown in Figure 14g.

The optical modulation of 28.5 d only appears in the MACHO, OGLE II, and first year of the OGLE III data where $I \sim 15.9$. But, when the source becomes brighter ($I \leq 15.2$) the modulation at 17.9 d starts to be seen in the light curve (Figure 15).

We note that the 28.5 d modulation disappears during and after the long type II outburst which lasts for about 1500 d even as the brightness of the source is returning to its quiescent state ($I \sim 15.9$). Both modulations are of low amplitude.

3.13 SXP22.1 (RX J0117.6-7330)

This was first discovered with ROSAT by Clark, Remillard, & Woo (1996) as an X-ray transient. Then, Charles, Southwell, & O'Donoghue (1996) identified its optical companion as a 14.2 mag OB star which was confirmed by Coe et al. (1998) as a Be(B1-2) star. The 22 s pulsation was found by Macomb et al. (1999).

After detrending the data by subtracting a linear fit, we found a peak at a period of 75.9 ± 0.06 d in its power spectrum (Figure 16b). The 75.9 d orbital outbursts appear to be strong when the source is brighter, and very weak at optical minima (Figure 16a). The folded light curve on this period is shown in Figure 16c. The long-term light curve is clearly variable on a timescale of ~ 2000 d, which is comparable to the duration of the dataset.

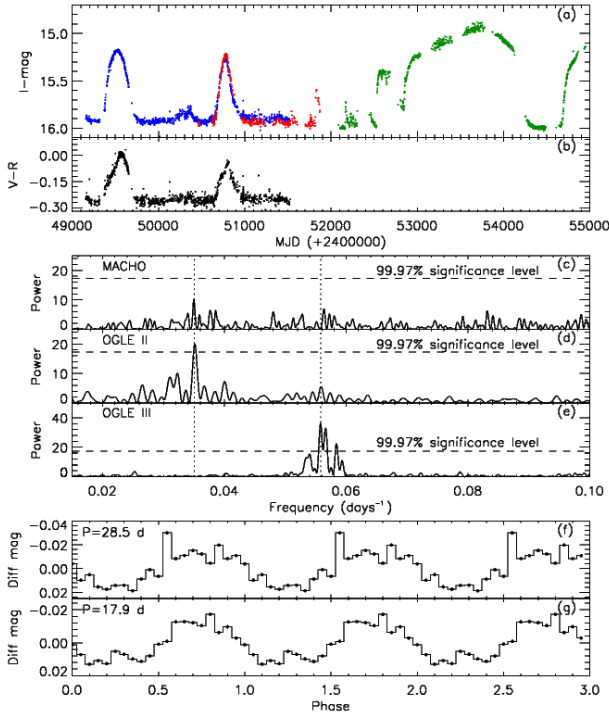


Figure 14. SXP18.3. (a): MACHO \mathcal{R} -band (blue), OGLE II (red) and OGLE III (green) light curves. (b): MACHO colour variation ($V - \mathcal{R}$). (c),(d),(e): Power spectrum of the detrended MACHO, OGLE II and second part of OGLE III data, respectively. (f),(g): The light curves folded on periods of 28.5 d and 17.9 d respectively.

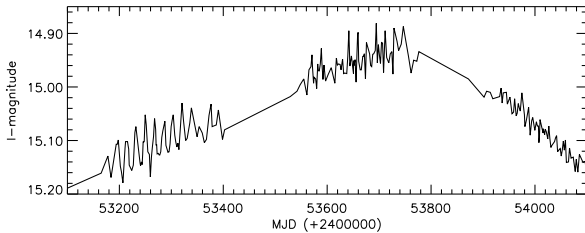


Figure 15. SXP18.3. Blow-up of the OGLE III light curve showing the 17.9 d modulation.

3.14 SXP25.5 (XMMU J004814.1-731003)

Lamb et al. (2002) found the 25.55 s pulsation of this X-ray source. The accuracy of its X-ray position with XMM allowed its optical companion to be identified as a $V=15.5$ star by Haberl et al. (2008b).

Analysis of the detrended OGLE III data reveals a significant peak at a period of 22.5 ± 0.005 d (Figure 17c). The 22.5 d period appears to be caused by several outbursts in the OGLE III data, and the folded light curve on this period shows a typical BeX outburst behaviour (Figure 17e).

We subdivided the OGLE III data into two parts, and then we folded it on the above period. The amplitude of the outbursts appear to vary as a function of brightness, they are weak when the source is brighter (first part of OGLE III data) and strong as the source becomes fainter (second part) (Figure 17d and 17e). Furthermore, the colour variation in

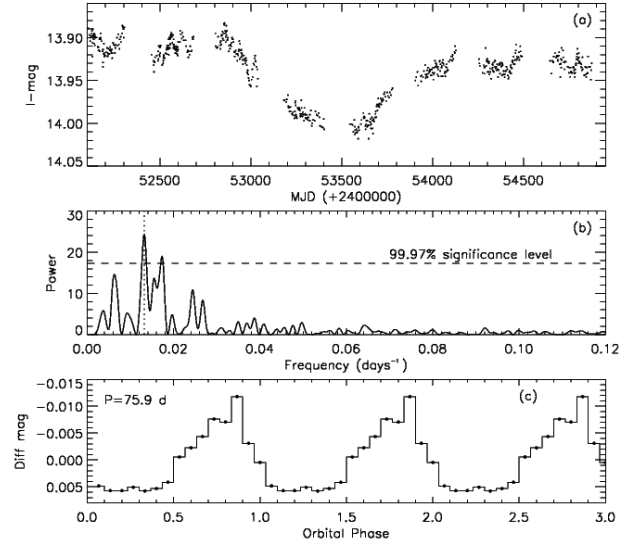


Figure 16. SXP22.1. (a): OGLE III light curve. (b): The power spectrum of the detrended OGLE III light curve showing the peak at $P = 75.9$ d. (c): The light curve folded on the orbital period of 75.9 d.

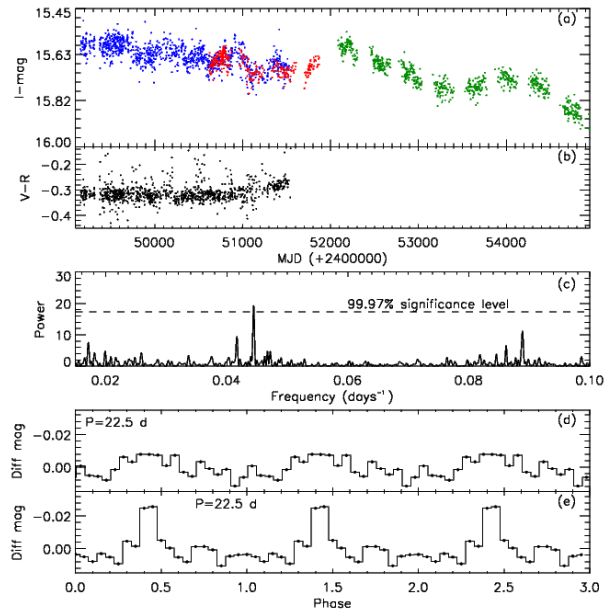


Figure 17. SXP25.5. (a): MACHO \mathcal{R} -band (blue), OGLE II (red) and OGLE III (green) light curves. (b): MACHO colour variation ($V - \mathcal{R}$). (c): Power spectrum of the OGLE III light curve. (d),(e): First (top) and second (bottom) part of the OGLE III light curve folded on the orbital period of 22.5 d.

Figure 17b shows a behaviour similar to that seen in A0538-66, where the source is bluer when brighter.

3.15 SXP31.0 (XTE J0111.2-7317)

SXP31.0 was first discovered with ASCA by Chakrabarty et al. (1998) as a 31s X-ray pulsar. Its optical companion was identified as a B0-B2 star by Coe, Haigh, & Reig (2000). Schmidtke & Cowley (2006)

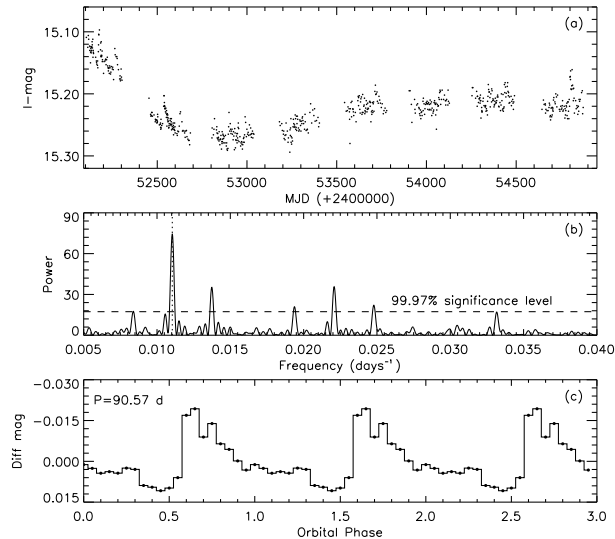


Figure 18. SXP31.0. (a) OGLE III light curve. (b): Power spectrum of the OGLE III light curve showing the peak at 90.57 d. (c): The OGLE III light curve folded on the orbital period of 90.57 d.

reported an orbital period of $P = 90.4$ d using OGLE III data.

After detrending the OGLE III light curve, we find a period of 90.57 ± 0.08 d, very similar to that already reported (Figure 18b). The light curve folded on this period is shown in Figure 18c. This classic BeX profile with outbursts every 90.57 d indicates that it is certainly the orbital period of SXP31.0. It is present even when the source is at optical minimum. Furthermore, the amplitude of the outbursts varies, being very strong during the two first years and one very strong outburst near the end of the OGLE III observations.

We do not find any long-term periodicity from the lightcurve (Figure 18a), although it is clearly variable on a timescale of ~ 2000 d.

3.16 SXP34.1 (CXOU J005527.9-721058)

The 34 s pulsation from this source was found by Edge, Coe, & McBride (2004) using Chandra data. The precise X-ray position led to an optical identification as a B-type star (Coe et al. 2005). The orbital period of SXP34.1 has not yet been reported.

The brightness of this BeX source is remarkably constant at $I \sim 16.82$ during all OGLE III observations (Figure 19a). However, its power spectrum shows a marginally significant peak at 598 ± 3.6 d (Figure 19b) with a very low amplitude.

However, we note that an orbital period of 598 d is too long for a 34 s BeX source based on the Corbet pulse/orbital period relationship.

3.17 SXP46.6 (1WGA J0053.8-7226)

Marshall, Lochner, & Takeshima (1997) initially reported a pulse period of 92 s from this source, but further analysis of the ASCA observations by Corbet et al. (1998) re-

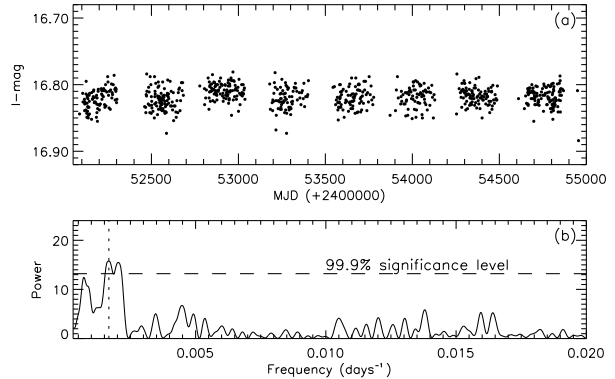


Figure 19. SXP34.1. (a): OGLE III light curve. (b) Power spectrum of the OGLE III light curve showing a significant peak at 598 d.

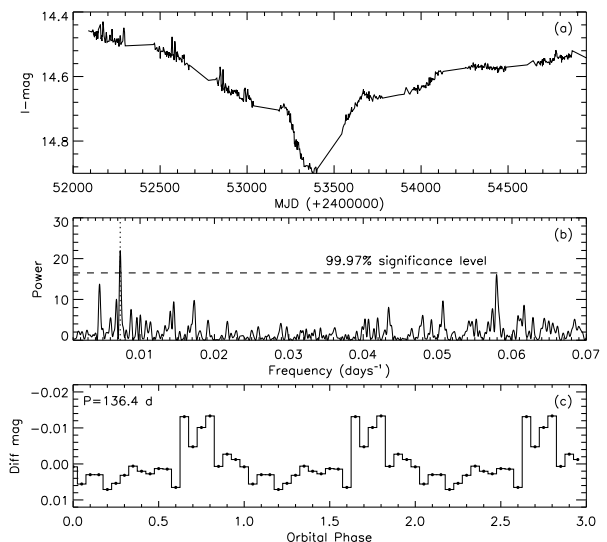


Figure 20. SXP46.6. (a): OGLE III light curve. (b): Power spectrum of the OGLE III light curve showing peaks at 136.4 d and 17.2 d. (c): The OGLE III light curve folded on 136.4 d.

vealed the period to be 46.63 ± 0.04 s. McGowan et al. (2008) confirmed its optical counterpart to be Star B from Buckley et al. (2001) with an optical orbital period of 136 ± 2 d (based on the data of Figure 20a), consistent with the X-ray period found by Galache et al. (2008).

The light curve of SXP46.6 shows not only one but two peaks for each periastron passage of the X-ray pulsar. The power spectrum of the detrended light curve reveals significant peaks at 136.4 ± 0.2 and 17.2 ± 0.003 d (Figure 20b). The light curve folded on 136.4 d is typical of BeX orbital behaviour, which is shown in Figure 20c. The 17.2 d appears to be the time interval between the two peaks in each orbital cycle.

We also find that the amplitude of the outbursts appears to become weaker as the source fades (Figure 20a). The OGLE III light curves show a large amplitude, long-term variation of about half a magnitude on timescales ~ 2000 d, comparable to the duration of the dataset.

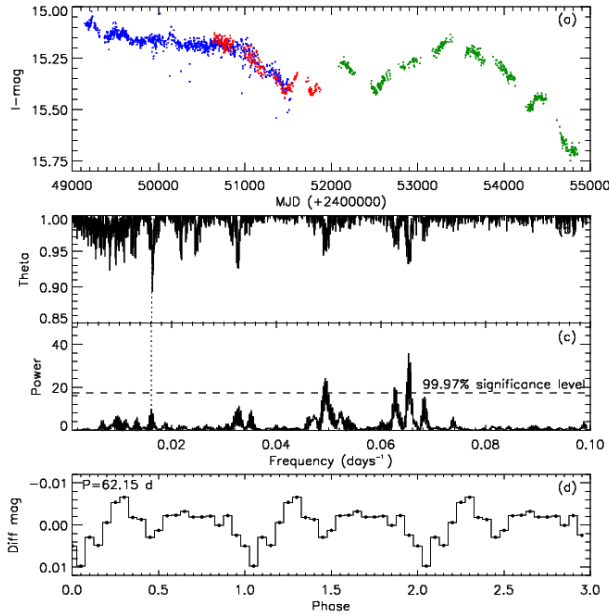


Figure 21. SXP59.0. (a): MACHO \mathcal{R} -band (blue), OGLE II (red) and OGLE III (green) light curves. (b): Power spectrum of the combined data showing peaks at 62.15 d period, and its harmonics at 15, 20, and 30 d. (c): Detrended combined light curve folded on the 62.15 d period.

3.18 SXP59.0 (XTE J0055-724)

This source was reported as a 59.0 ± 0.2 s X-ray pulsar by Marshall et al. (1998). Its optical companion is identified as MA[93]810 and MACHO 207.16259.23. Schmidtke & Cowley (2005b) reported an orbital period of 60.2 d in the OGLE II data. However, Galache et al. (2008) suggested an X-ray orbital period of 122.1 ± 0.38 d in their RXTE data.

The power spectrum (PDM and L-S) of our detrended MACHO and OGLE combined lightcurve has a significant peak at 62.15 ± 0.04 d, consistent with that previously reported, and its harmonics at 15, 20, and 30 d (Figure 21b, and 21c). We note that Galache et al. (2008) found an X-ray period of 122 d which is about twice our value. The light curve folded on 62.15 d is shown in Figure 21d. The long-term light curve exhibits a large amplitude (> 0.5 mag) variability on a timescale of ~ 3000 d.

3.19 SXP74.7 (AX J0049-729)

The 74.7 s pulsation from AX J0049-729 was discovered by Yokogawa & Koyama (1998d). Schmidtke & Cowley (2005b) reported an orbital period of 33.4 ± 0.4 d in the MACHO lightcurve of this source.

The power spectrum of the detrended light curve of the complete MACHO and OGLE observations shows a very significant peak at a period of 33.38 ± 0.01 d (Figure 22b), similar to that already reported. The light curve folded on this period is shown in Figure 22d.

The power spectrum of the long-term light curve shows a peak at 1220 ± 64 d (Figure 22c), and the light curve folded on this period is shown in Figure 22e.

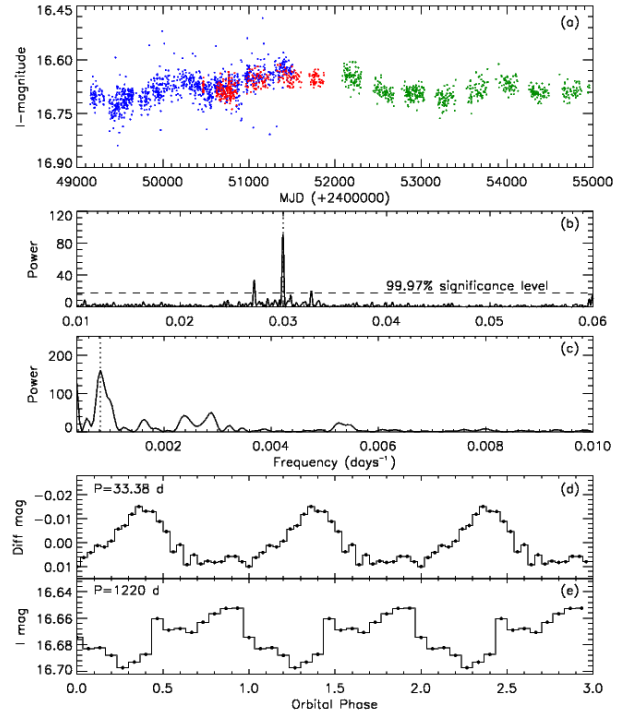


Figure 22. SXP74.7. (a): MACHO \mathcal{R} -band (blue), OGLE II (red) and OGLE III (green) light curves. (b) and (c): Power spectrum of the detrended and combined light curve showing peaks at 33.38 d and 1220 d. (d) and (e): The light curves folded on 33.38 d and 1220 d period.

3.20 SXP82.4 (XTE J0052-725)

Corbet et al. (2002) first observed the pulse period of 82.4s for this X-ray pulsar with RXTE. Its position was determined from Chandra data by Edge et al. (2003b).

Its long-term light curve appears to be constant until $\text{MJD} \sim 50800$, following which it shows a dramatic variation on timescales ~ 2000 d, and declining by ≥ 1 mag (see Figure 23a).

Schmidtke & Cowley (2005b) have studied the MACHO dataset but were unable to find any signature of its orbital period. However, Galache et al. (2008) reported an X-ray period of ~ 362.3 d, and derived the X-ray outburst ephemeris.

We have split the OGLE III datasets into two parts. The power spectra (PDM and L-S) of both parts show a significant peak at 171 ± 0.3 d, which is less than half the reported X-ray period (Figure 23b). The PDM shows a peak at 370.2 d, very similar to the previously reported X-ray period, but it may be caused by the annual sampling of the data. The light curve folded on the 171 d period is shown in Figure 23d.

3.21 SXP91.1 (RX J0051.3-7216)

The 91.12 s pulse period of this X-ray pulsar was reported by Corbet et al. (1998). Stevens, Coe, & Buckley (1999) proposed its optical counterpart as an $\text{H}\alpha$ emitting object MA[93]413 (Schmidtke et al. 2004). An orbital period of

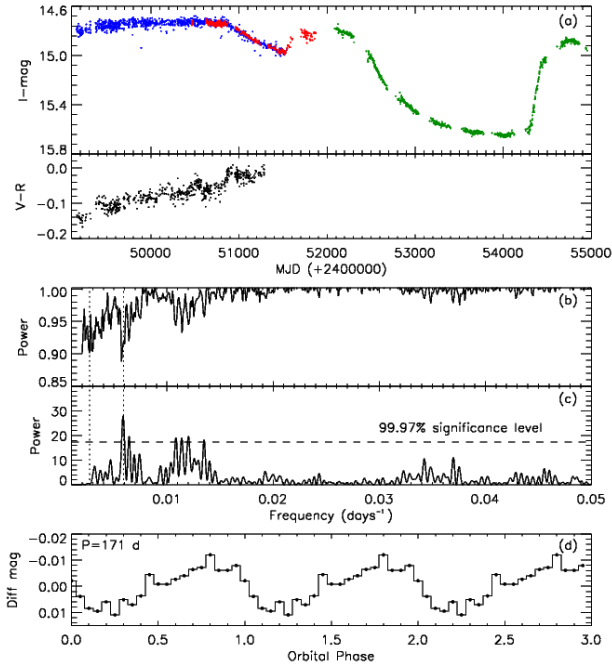


Figure 23. SXP82.4. (a): MACHO \mathcal{R} -band (blue), OGLE II (red) and OGLE III (green) light curves. (b) and (c): Power spectra (PDM and L-S) of the OGLE III light curve showing a significant peak at 171 d, the vertical dashed line represents the previously reported period. (d): The OGLE III light curve folded on the 171 d period.

88.25 d was found by Schmidtke et al. (2004) in the MACHO light curve.

The power spectrum of the detrended light curves reveals a very significant peak at 88.3 ± 0.1 d (Figure 24b). The folded light curve on the 88.3 d period is shown in Figure 24c. The combined long-term light curve varies on timescales of ~ 4000 d. Moreover, the amplitude of the 88.3 d outbursts was clearly variable throughout this 4000 d cycle, appearing stronger when the source brightens (Figure 24a).

3.22 SXP101 (AX J0057.4-7325)

This variable X-ray source was found to be a 101.45 s X-ray pulsar by Yokogawa et al. (2000a). McGowan et al. (2007) confirmed its optical counterpart as a $V = 14.9$ star with a period (presumed to be orbital) of 21.9 d in both MACHO and OGLE III light curves.

We detrended the complete MACHO and OGLE III datasets and found a peak consistent with the previously reported period at 21.95 ± 0.004 d (Figure 25b). The light curve folded on this period is shown in Figure 25d. The power spectrum of the combined light curve of SXP101 also shows peaks at 758 ± 6 d and 355 d (Figure 25c). The peak at 355 d is due to the data sampling. The folded light curve on the 758 d period is shown in Figure 25e.

3.23 SXP138 (CXOU J005323.8-722715)

The 138.04 s pulse period of this source was reported by Edge, Coe, & McBride (2004) using archival Chandra data.

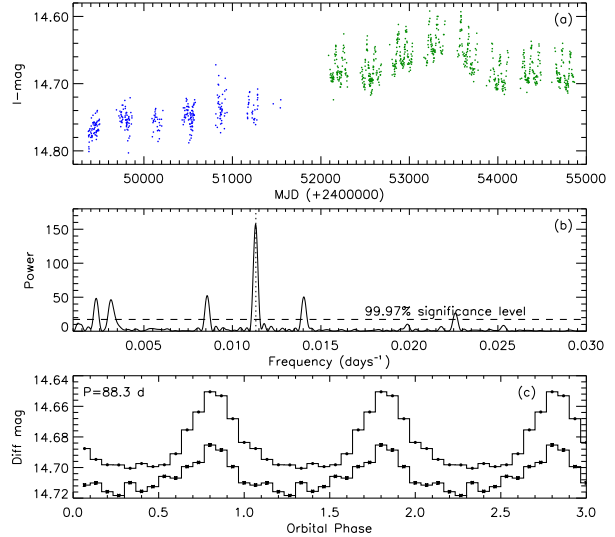


Figure 24. SXP91.1. (a): MACHO \mathcal{R} -band (blue), and OGLE III (green) light curves. (b): Power spectrum of the combined detrended light curves showing a peak at 88.3 d. (c): OGLE III and MACHO light curves folded on 88.3 d.

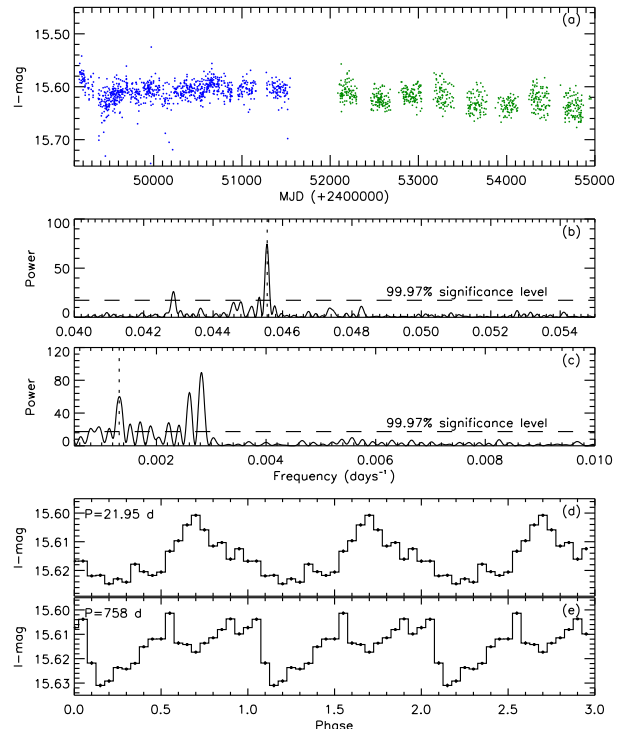


Figure 25. SXP101. (a): MACHO \mathcal{R} -band (blue), and OGLE III (green) light curves. (b) and (c): Power spectrum of the combined MACHO and OGLE light curves showing a significant peak at 21.95 d and 758 d. (d) and (e): The combined light curve folded on 21.95 d and 758 d period, respectively.

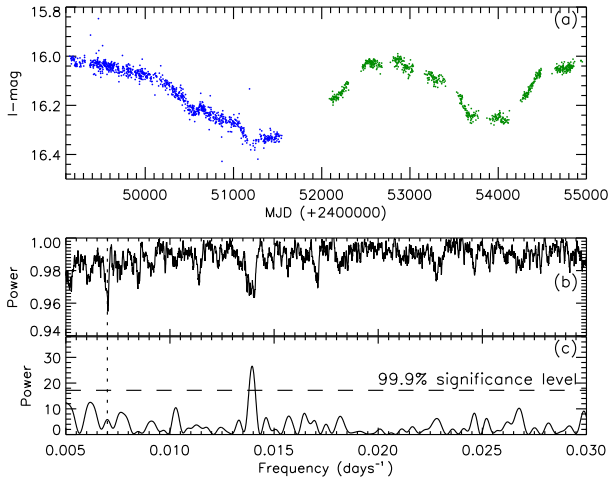


Figure 26. SXP138. (a): MACHO \mathcal{R} -band (blue), and OGLE III (green) light curves. (b) and (c): Power spectrum (PDM and L-S) of the detrended light curve with a peak at $P=143$ d.

It was identified with MA[93]667 and found to have a period of ~ 125 d in MACHO data (Edge 2005a). This was confirmed by Schmidtke & Cowley (2006) who found a period of 122-123 d.

The L-S power spectrum of the detrended MACHO and OGLE III data shows a significant peak at 71.8 ± 0.1 d, however the deepest peak in the PDM occurs at twice this value, 143 ± 0.2 d (Figure 26b, and 26c). We found a very weak peak at 125 d, but in the MACHO data only.

The long-term light curve shows a large variation of about 0.4 mag with a period of 2700 d.

3.24 SXP140 (XMMU J005605.2-722200)

Sasaki, Pietsch, & Haberl (2003) discovered this 140 s pulsar in XMM-Newton observations, whose accurate X-ray position clearly identifies it with MA[93]904. Schmidtke & Cowley (2006) found a 197 ± 5 d period in a segment of MACHO light curve (MJD 49650-50500) which they suggested as the orbital period.

The light curves show large amplitude, long-term variations of half a magnitude, but the power spectrum of the OGLE III light curve reveals nothing significant at the previously reported orbital period. However, it does show a very strong peak at 492 ± 2.4 d (Figure 27c), and the combined light curve folded on this period is shown in Figure 27d.

Figure 27b shows the colour variation MACHO $\mathcal{V} - \mathcal{R}$ which correlates closely with the flux modulation. A lag between the MACHO colour and brightness variation is also seen at its optical maximum.

3.25 SXP172 (RX J0051.9-7311)

The optical counterpart of this source was identified as a Be star by Cowley et al. (1997), and is also known as MA[93]504. Subsequently, Yokogawa et al. (2000b) found an X-ray pulsation with a period of 172.4 s, which was refined by Haberl & Pietsch (2004) to 172.21 ± 0.13 s. Laycock et al. (2005) reported a 67 ± 5 d period based on several X-ray outbursts. An orbital period of 69.9 ± 0.6 d was proposed by

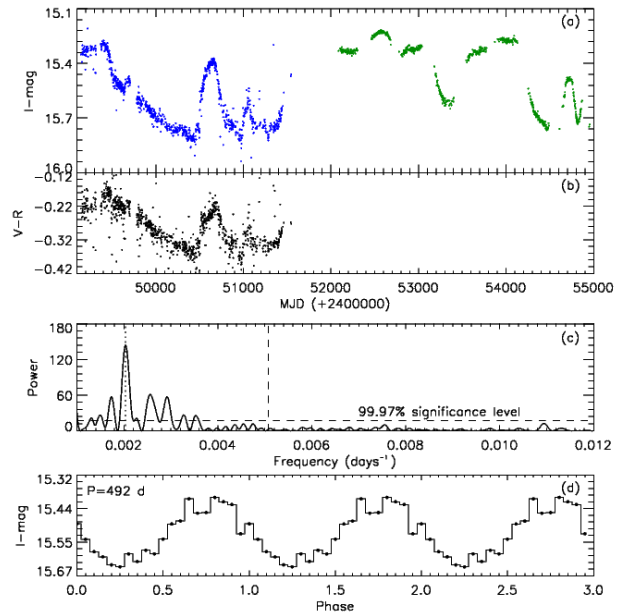


Figure 27. SXP140. (a) MACHO \mathcal{R} -band (blue), and OGLE III (green) light curves. (b): MACHO colour variation $\mathcal{V} - \mathcal{R}$. (c): Power spectrum of the combined light curve with a highest peak at 492 d, the vertical dash line represents the frequency of the previously reported period. (d): The combined light curves folded on the period of 492 d.

Schmidtke & Cowley (2006) using only the first two years of the OGLE II data (which they named Segment A).

Our power spectrum of the detrended OGLE II light curve shows a peak at 67.9 ± 0.04 d (Figure 28b), close to that previously reported. However, the OGLE III power spectrum (Figure 28c) does not show a peak at this period. The folded OGLE II light curve on the 67.9 d period is shown in Figure 28d. The long-term light curve shows a large amplitude variation on a timescale of ~ 2000 d (Figure 28a).

3.26 SXP202A (1XMMU J005921.0-722317)

Majid, Lamb, & Macomb (2004) discovered the 202 s pulsation of this X-ray source in a number of archival XMM-Newton observations. The optical counterpart was identified as MACHO 207.16545.12.

The light curve is highly variable by ≥ 0.5 mag, and the power spectrum of the combined light curves revealed strong low frequency power with a peak at $P=1220 \pm 61$ days (Figure 29e). The folded lightcurve on this long-term period is shown in Figure 29g. In Figure 29b, we can see that the optical maxima and the peaks of the colour variation (MACHO $\mathcal{V} - \mathcal{R}$) are not synchronized.

Using the RXTE/PCA observation, Galache et al. (2008) reported that they did not find any clear orbital period in the data for SXP202. However, they noted that the time interval between the six X-ray maxima detected since MJD 53000 is about ~ 91 d. After detrending the optical data from MACHO and OGLE observations, we found a peak at 71.9 ± 0.05 d and several peaks at its harmonics (36 d, 23 d, and 18 d) in both PDM and L-S power spectra (Fig-

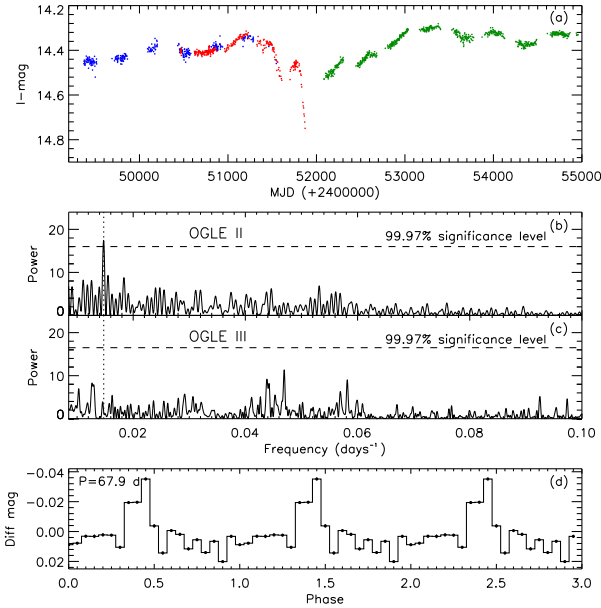


Figure 28. SXP172. (a): MACHO \mathcal{R} -band (blue), OGLE II (red) and OGLE III (green) light curves. (b) and (c): Power spectrum of the detrended OGLE II (peak at $P=67.9$ d) and OGLE III light curves, the vertical dotted line represents the frequency of the previously reported 69.9 d orbital period. (d): The folded OGLE II light curve on the 67.9 d period

ure 29c and 29d). The detrended light curve folded on this period is complex (Figure 29f).

3.27 SXP202B (XMMU J005929.0-723703)

XMMU J005929.0-723703 was reported as a new X-ray pulsar with a pulse period of 202 s by Haberl, Eger, & Pietsch (2008a). They identified its optical companion with a $V=14.9$ Be star (also MA[93]1147), and classified it as a B0-5(III)e in the 2dF survey of the SMC.

Its light curves show large amplitude (~ 0.5 mag) variations on a timescale of ~ 3000 d (Figure 30a). The power spectra (PDM and L-S) of the detrended light curve show peaks at $P = 224 \pm 0.5$ d and its harmonic 113 d (Figure 30b and 30c). The highest peak in the PDM is at $P = 224$ d, which is consistent with the time interval between consecutive outbursts in Figure 30a.

The 224 d modulation appears as a sequence of outbursts during the last five years of the OGLE III observations. Furthermore, the folded light curves on the period of 224 d shows a classic BeX outburst profile (Figure 30d), which suggests that the 224 d period is orbital. This period is in good agreement with the Corbet (1984) $P(\text{pulse})/P(\text{orbit})$ relation.

The amplitude of outbursts is clearly variable (Figure 30d) and appears larger when the source is brighter, and either lower or even absent when fainter (see Section 4, Figure 43).

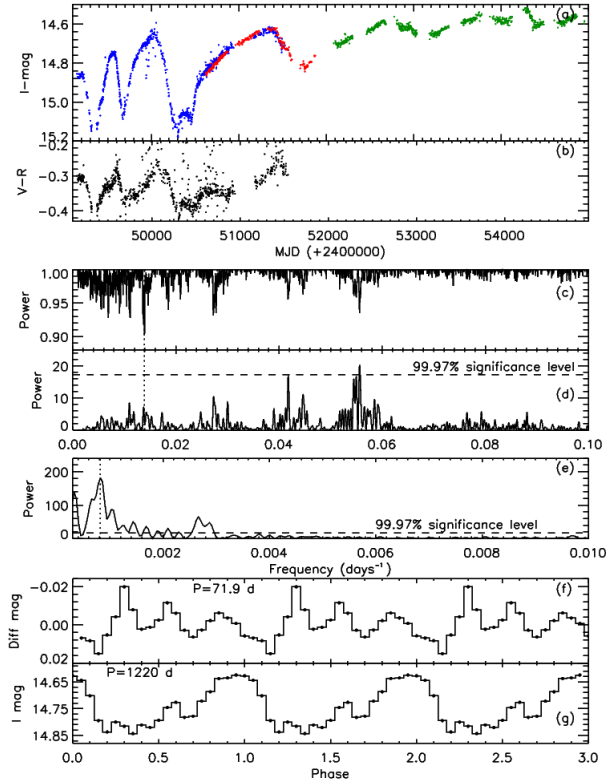


Figure 29. SXP202A. (a): MACHO \mathcal{R} -band (blue), OGLE II (red), and OGLE III (green) light curves. (b): MACHO colour variation $V - \mathcal{R}'$. (c) and (d): PDM and L-S periodogram of the detrended light curve showing a peak at 71.9 d and its harmonics. (e): Power spectrum of the combined light curve with a peak at $P=1220$ d. (f) and (g): The light curves folded on the 71.9 d, and 1220 d periods.

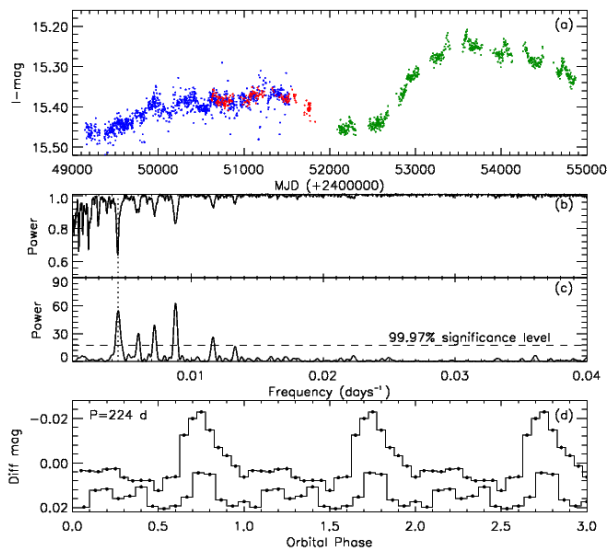


Figure 30. SXP202B. (a): MACHO (blue), OGLE II (red), and OGLE III (green) light curves. (b) and (c): Power spectra (PDM and LS) of the OGLE III light curve showing peak at 224 d. (d): The OGLE III light curve folded on 224 d period at optical maxima and minima.

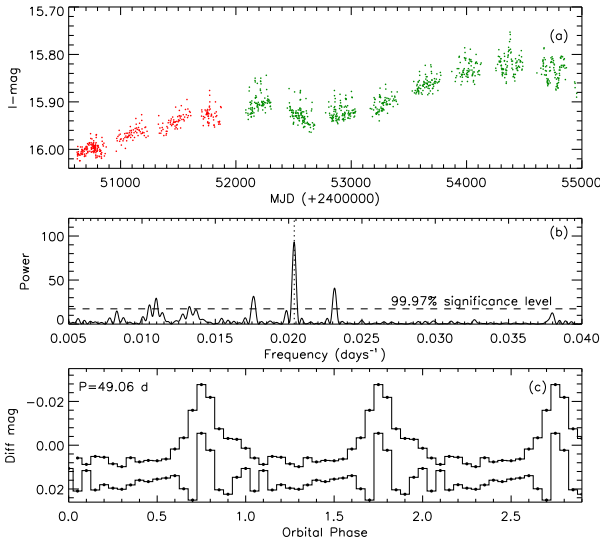


Figure 31. SXP264. (a): OGLE II, and OGLE III light curves. (b): Power spectrum of the detrended light curve showing a peak at 49.06 d. (c): OGLE II and OGLE III light curves folded on the 49.06 d orbital period.

3.28 SXP264 (RX J0047.3-7312)

The 264 ± 1 s pulsations were discovered by Ueno et al. (2004), whose accurate XMM-Newton location allowed its optical counterpart to be identified clearly as a Be star MA[93]172. It also appears in MACHO (MACHO 212.15792.77) and OGLE catalogues of variable stars. Schmidtke & Cowley (2005b) reported an orbital period of 49.1 d in OGLE data.

Analysis of the detrended light curve reveals a significant peak at 49.06 ± 0.02 d, consistent with that previously reported (Figure 31b). The light curve folded on this period is shown in Figure 31c. The combined light curve is clearly variable on a timescale of ~ 2000 d with an increase in brightness over the last ~ 5000 d (Figure 31a). The amplitude of the 49 d orbital outburst increases with its brightness.

3.29 SXP280 (RX J0057.8-7202)

The optical counterpart of this 280.4 s X-ray pulsar is identified as the Be star MA[93]1036. Its long-term light curve shows a clear series of outbursts every 127.3 d (Schmidtke & Cowley 2006). The power spectrum of the detrended light curve is dominated by a peak consistent with this at 127.5 ± 0.2 d (Figure 32b).

We split the OGLE III data into two parts. Figure 32c represents these two parts of the OGLE III light curve folded on the 127.5 d period. The outburst amplitude of SXP280 also varies significantly (~ 0.25 mag) on a timescale of ~ 2000 d.

3.30 SXP293 (RX J0058.2-7231)

Corbet et al. (2004b) detected the 292.9 ± 0.4 s pulsations in RXTE observations of the SMC. The optical counterpart was identified as a Be star by Schmidtke et al. (1999). Galache et al. (2008) suggested an orbital period of 151 d

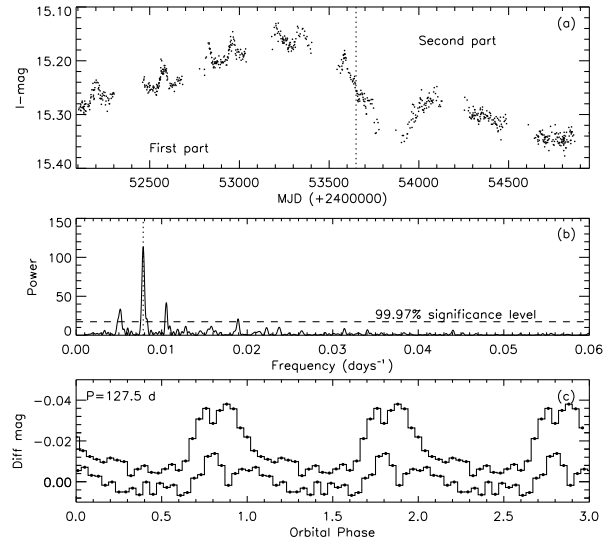


Figure 32. SXP280. (a): OGLE III light curve. (b): Power spectra of the detrended light curve with a peak at 127.5 d. (c): First and second half of the OGLE III light curve folded on the 127.5 d period.

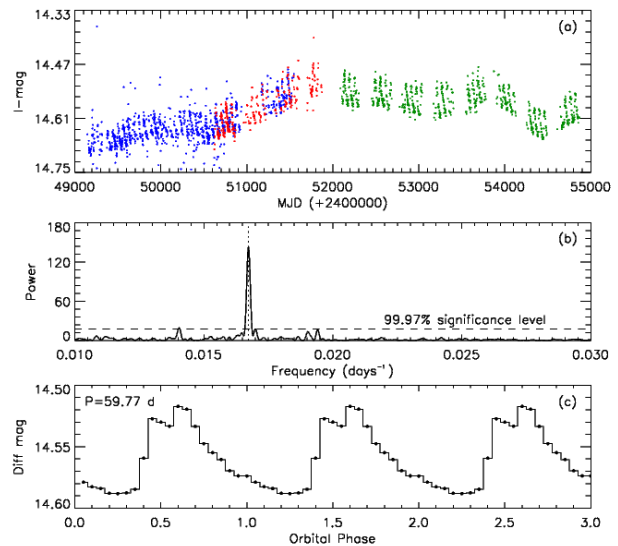


Figure 33. SXP293. (a): MACHO (blue), OGLE II (red), and OGLE III (green) light curves. (b): Power spectrum of the combined light curve showing a peak at 59.77 d period. c) The light curve folded on the 59.77 d period.

in their X-ray data from RXTE observation. However, both MACHO and OGLE light curves show clearly the orbital modulation with a period of $P = 59.72$ d, which appears as a series of very regular outbursts.

The combined light curves from MACHO and OGLE observations are shown in Figure 33a, and SXP293 shows a substantial increase in brightness until the end of the OGLE II observations. The power spectrum of the combined light curves shows a significant peak at a period of 59.77 ± 0.03 d (Figure 33b), and the folded light curve on this period shows a double peaked classical BeX profile (Figure 33c). The long-term light curve is variable on a timescale of ~ 2500 d

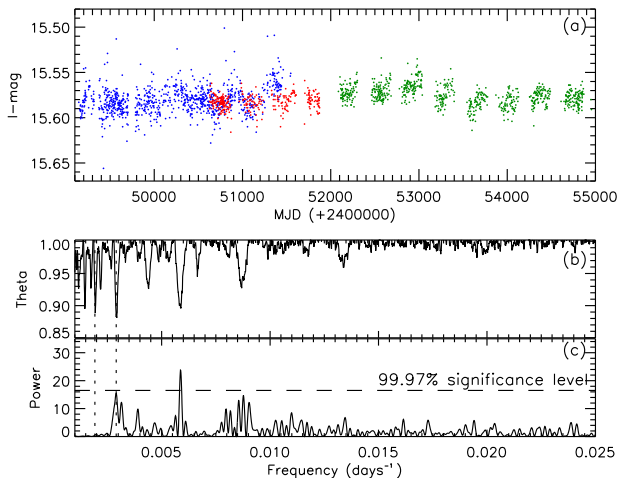


Figure 34. SXP304. (a): MACHO (blue), OGLE II (red), and OGLE III (green) light curves. (b) and (c): PDM and L-S periodograms of the combined light curves showing a peak at 344 d, the dashed lines represent the 344 d and the previously reported 520 d.

3.31 SXP304 (RX J0101.0-7206)

This 304.49 s X-ray pulsar was discovered in Chandra observations by Macomb et al. (2003). Its X-ray position is coincident with the emission-line star MA[93]1240. Schmidtke & Cowley (2006) suggested a possible orbital period of 520 ± 12 d in the MACHO data.

The power spectrum of the extended detrended dataset plotted in Figure 34c shows peaks at 344 ± 1.2 d (deepest peak in the PDM) and its harmonic 170 ± 0.3 d. The previously reported period 520 d appears as a peak in the PDM statistic of the combined data, but its power is lower than the 344 d period (Figure 34b).

3.32 SXP327 (XMMU J005252.1)

The pulsation of 327 s was discovered in the Chandra observations of the SMC by Laycock, Zezas, & Hong (2008). Its precise X-ray position allows the optical companion to be identified with object 207.16147.60 in the MACHO catalogue, and SMC101.4 25097 in the OGLE III catalogue. Udalski & Coe (2008) reported its orbital period to be 45.995 d using MACHO and OGLE III data.

The MACHO light curve shows only a gradual fading, but the OGLE III light curve appears variable on longer timescales. The power spectrum of OGLE III data reveals peaks at 1274 ± 143 d and the orbital period $P = 45.9 \pm 0.2$ d (Figure 35b and 35c). The folded light curve on the orbital period (Figure 35d) shows a classic BeX profile, with an outburst amplitude of ~ 0.25 mag. In addition, the orbital lightcurve shows a secondary maximum, which can arise due to misalignment between the circumstellar disc and the orbital plane of the neutron star.

3.33 SXP348 (AX J0103-722)

A 345.2 s pulsation was first detected in the BeppoSAX observation of AX J0103-722 in the SMC in 1998 by

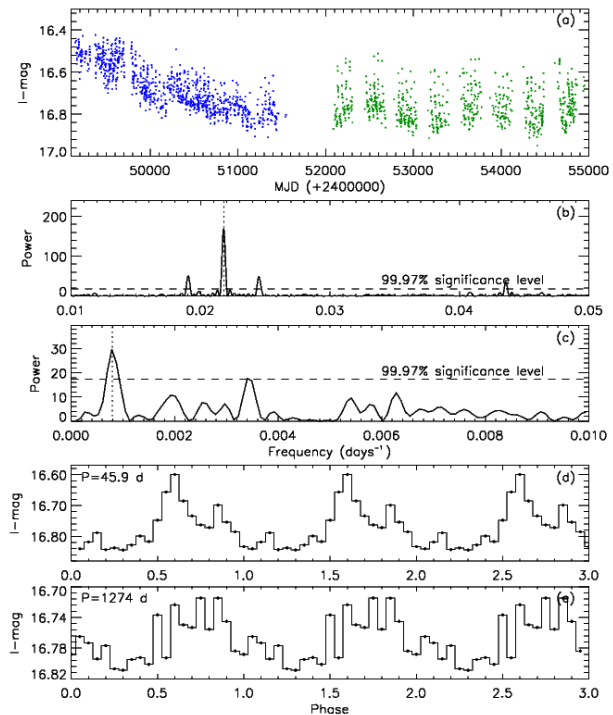


Figure 35. SXP327. (a): MACHO \mathcal{R} -band (blue), and OGLE III (green) light curves. (b) and (c): Power spectra of the combined light curve showing peaks at the presumed orbital period of 45.9 d, and 1274 d. (d) and (e): The combined light curves folded on 45.9 d and 1274 d respectively.

Israel et al. (1998), then Yokogawa & Koyama (1998b) reported a pulse period of 348.9 s in the 1996 ASCA observation of the same source. The X-ray position from Chandra is coincident with a 14.8 mag Be star (Hughes & Smith 1994) which is in the catalogue of Meyssonier & Azzopardi (1993) as MA[93]1367. Schmidtke & Cowley (2006) suggested an orbital period of 93.9 d based on the OGLE II data.

The power spectrum of our detrended OGLE II light curve shows a peak at 94.4 ± 0.1 d (Figure 36b), very close to that previously reported. However, its power in the L-S periodogram of the OGLE III data is very low (Figure 36c). The OGLE II data folded on the orbital period of 94.4 d is shown in Figure 36d, but we note that the modulation amplitude is low. The source has faded dramatically recently (Figure 36a). The long-term lightcurve varies on a timescale of ~ 2000 d (Figure 36a).

3.34 SXP455 (RX J0101.3-7211)

Sasaki et al. (2001) discovered the 455 ± 2 s pulsations in XMM-Newton EPIC-PN data of RX J0101.3-7211. Its optical counterpart was suggested to be MA[93]1257 (Haberl & Sasaki 2000), and optical observations by Sasaki et al. (2001) confirmed its Be nature. An orbital period of 74.7 d was found by Schmidtke et al. (2004) and confirmed by Coe et al. (2005).

The light curve of SXP455 displays a substantial long-term variation with a period of 1886 ± 145 d (see power spectra in Figure 37e). The light curve folded on this superorbital period is shown in Figure 37g.

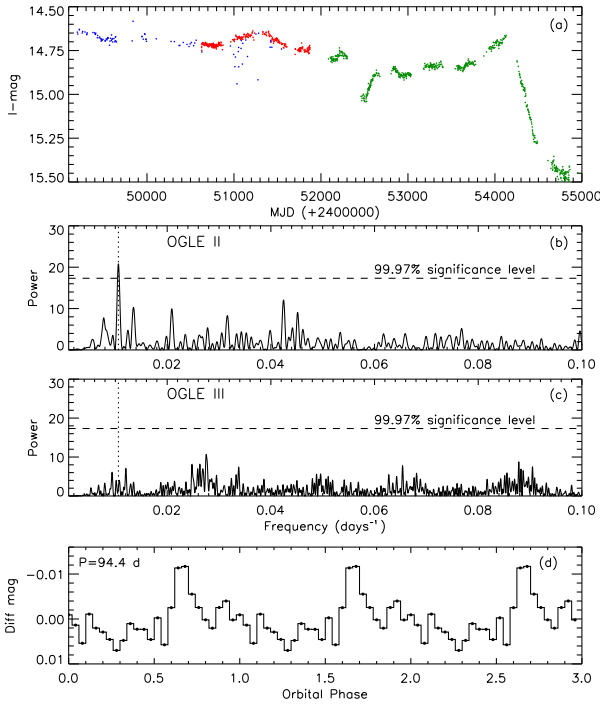


Figure 36. SXP348. (a): MACHO \mathcal{R} -band (blue), OGLE II, and OGLE III (green) light curves. (b): Power spectrum of the OGLE II light curve showing a significant peak at 94.4 d. (c): Power spectrum of the OGLE III light curve. (d): The folded OGLE II light curve on the 94.4 d period.

The power spectrum of our detrended OGLE II light curve (Figure 37c) shows a peak at the 74.96 ± 0.05 d orbital period. Remarkably, this periodicity appears absent in the OGLE III light curve (Figure 37d). The OGLE II and OGLE III light curves folded on this period are shown in Figure 37f and that of OGLE II exhibits a classic BeX outburst profile with a secondary peak.

3.35 SXP504 (AX J0054.8-7244)

The pulse period of SXP504 was independently discovered in Chandra archival data by Edge, Coe, & McBride (2004) with a period of ~ 500 s and in XMM-Newton data by Haberl et al. (2004) with a period of 499.2 ± 0.7 s. The precise X-ray position is coincident with an emission-line star MA[93]809 which is the same star as 207.16254.16 in the MACHO catalogue. Edge, Coe, & McBride (2004) reported a period of 268.6 ± 0.1 d in the MACHO and OGLE II data, which was presumed to be orbital.

The MACHO and OGLE light curves show clearly the regular optical outbursts at ~ 270 d intervals. After detrending the MACHO and OGLE light curves, we computed their power spectra. A peak at 272 ± 0.7 d was found in both MACHO, OGLE II and OGLE III data, which is consistent with the presumed orbital period (Figure 38b and 38c). The folded OGLE III light curve on this period is shown in Figure 38e, which has the same profile as the MACHO folded light curve reported by Edge, Coe, & McBride (2004).

The light curve exhibits a smooth long-term quasi-periodic modulation on a timescale of 3500 d. Accordingly,

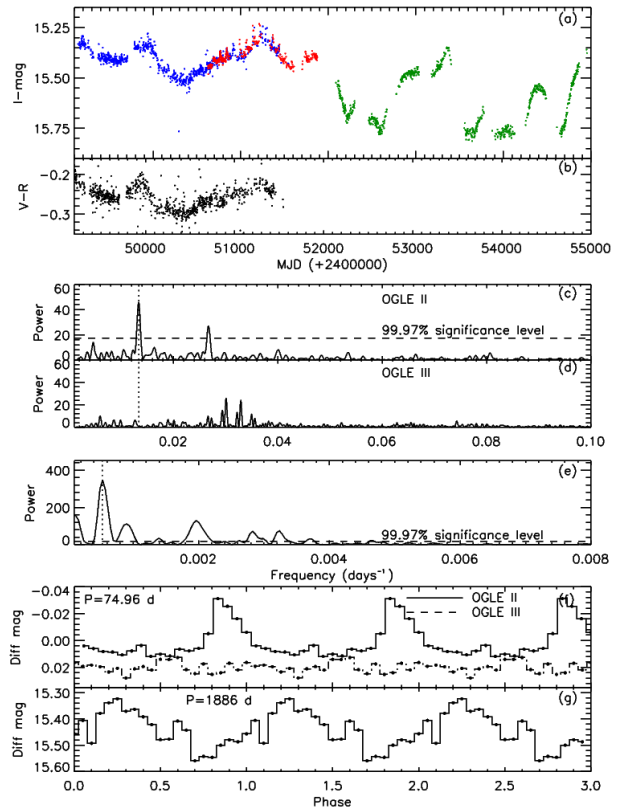


Figure 37. SXP455. (a): MACHO \mathcal{R} -band (blue), OGLE II (red), and OGLE III (green) light curves. (b): MACHO colour variation $\mathcal{V}-\mathcal{R}$. (c), (d), and (e): Power spectrum of the detrended OGLE II, OGLE III and combined light curves showing peaks at 74.96 d and 1886 d respectively. (f) and (g): Folded light curve on the presumed orbital and superorbital periods.

the L-S periodogram and PDM reveals very strong low-frequency power with a peak at 3448 ± 119 d (Figure 38d).

3.36 SXP565 (CXOU J005736.2-721934)

Macomb et al. (2003) discovered the 564.8 s pulsations of this source with Chandra. The optical counterpart was identified as an emission-line star, [MA93] 1020 in the Meyssonnier & Azzopardi (1993) catalogue, and a period of 95.3 d was found by Schmidtke et al. (2004). However, using RXTE/PCA observations, Galache et al. (2008) reported a period of 151.8 d.

To try to determine the real orbital period of the system, we have detrended the OGLE III data. Analysis of the detrended light curve reveals a peak at 152.4 ± 0.2 d (Figure 39b), which appears to be caused by several BeX-type outbursts in the light curve. The folded light curve on this period (Figure 39c) shows a profile similar to those seen in other BeX sources. This suggests that the 152.4 d period is the real orbital period of SXP565 which is in good agreement with the X-ray period of 151.8 d found by Galache et al. (2008).

The combined long-term light curve (Figure 39a) shows a very clear quasi-periodic variation on a timescale of ~ 3000 d.

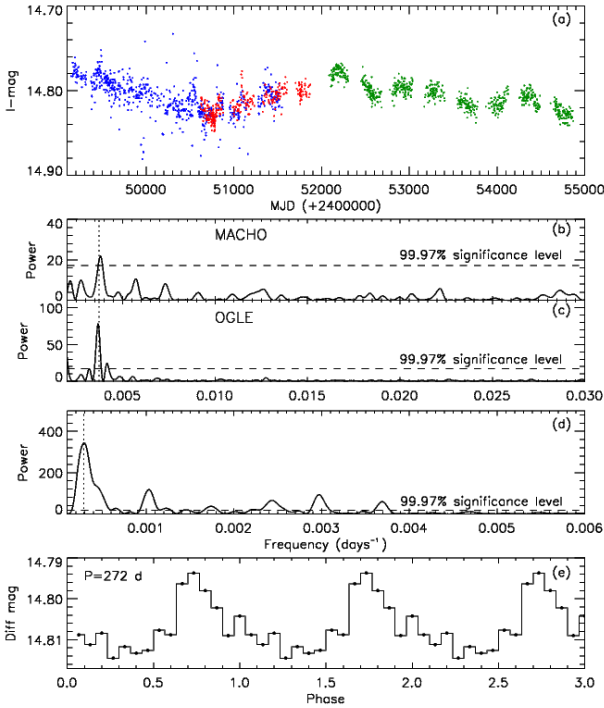


Figure 38. SXP504. (a): MACHO \mathcal{R} -band (blue), OGLE II (red), and OGLE III (green) light curves. (b) and (c): Power spectrum of the MACHO and OGLE III data showing a peak at 272 d. (d): Power spectrum of the combined light curve with a peak at 3448 d. (e): The folded light curve on the 272 d presumed orbital period.

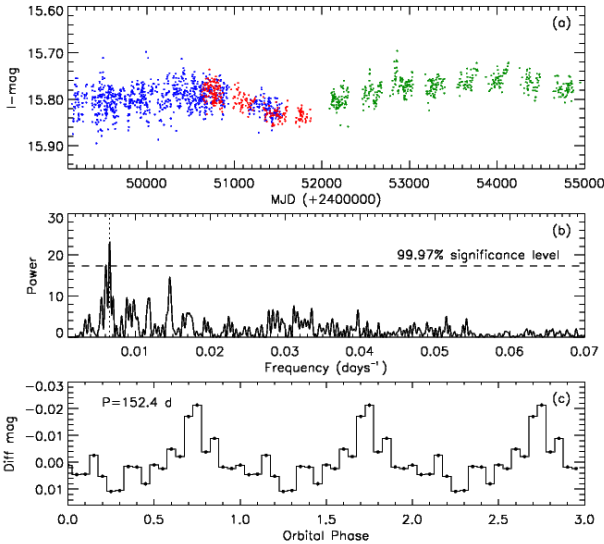


Figure 39. SXP565. (a): MACHO \mathcal{R} -band (blue), OGLE II (red) and OGLE III (green) light curves. (b): Power spectrum of the detrended light curves showing a significant peak at 152.4 d period. (c): The detrended light curve folded on the presumed 152.4 d orbital period.

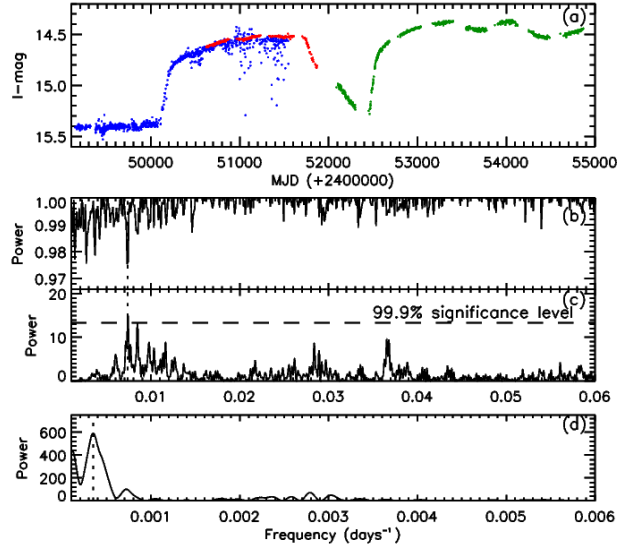


Figure 40. SXP645. (a): MACHO \mathcal{R} -band (blue), OGLE II (red) and OGLE III (green) light curves. (b), (c), and (d): Power spectrum (PDM and L-S) of the detrended and combined light curves showing peaks at 135.4 d and 2857 d.

3.37 SXP645 (XMMU J005535.2-722906)

This transient X-ray source was detected with a pulse period of 645 s by Haberl, Eger, & Pietsch (2008a). They identified the optical counterpart as a $V \sim 14.6$ star which is object 207.16315.28 in the MACHO catalogue, and SMC-SC7 137527 in OGLE II.

The long-term light curves show very large amplitude (~ 1 mag) variations repeating after ~ 2500 d (Figure 40a), which causes a strong low-frequency peak at 2857 ± 81 d in the power spectrum (Figure 40d).

At higher frequency, we found a significant peak at 135.4 ± 0.5 d in the PDM and L-S power spectrum (Figure 40b and 40c), which could be the orbital period of SXP645.

3.38 SXP701 (XMMU J005517.9-723853)

Haberl et al. (2004) discovered 701.6 ± 1.4 pulsations from this source during an XMM-Newton Target of Opportunity (ToO) observation of the SMC field around XTE J0055-727. This X-ray source is identified with MACHO 207.16313.35 and OGLE II SMC-SC7 129062. Schmidtke & Cowley (2005b) found a weak 412 d modulation in the MACHO data.

The power spectra (PDM and L-S) of our OGLE III light curve reveals a significant peak at 412 ± 5 d, which is the presumed orbital period (Figure 41b, 41c), very close to that found in MACHO data by Schmidtke & Cowley (2005b). The folded light curve on this period is shown in (Figure 41d).

The long-term light curves do not show periodic variability other than the presumed orbital period, but a gradual fading over ~ 5000 d (Figure 41a) is evident.

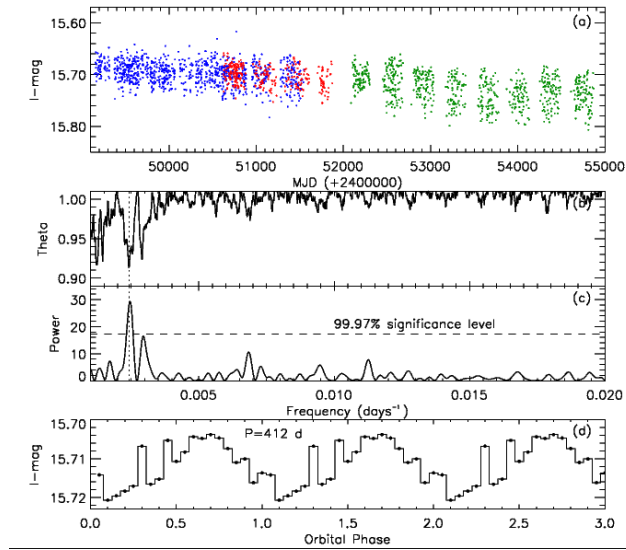


Figure 41. SXP701. (a): MACHO \mathcal{R} -band (blue), OGLE II (red) and OGLE III (green) light curves. (b) and (c): Power spectrum (PDM and L-S) of the detrended combined light curves showing a significant peak at 412 d period. (c): The detrended light curve folded on the 412 d period.

3.39 SXP755 (RX J0049.7-7323)

Yokogawa et al. (2000c) discovered 755.5 ± 0.6 s pulsations in an ASCA observation of AX J0049.5-7323. The optical counterpart was identified as a $V=15$ star by Edge & Coe (2003a), and is designated [MA93] 315. The X-ray period of 396 ± 5 d was found by Laycock et al. (2005) and is consistent with the optical period of ~ 394 d reported by Schmidtke et al. (2004).

The light curve of SXP755 shows a series of outbursts which appear to strengthen as the source brightens (Figure 42a). The power spectrum (PDM and L-S) of the detrended combined light curve shows a peak at 391 ± 2 d (Figure 42b, 42c), very close to the presumed orbital period. The folded light curve on this period is shown in Figure 42d.

The combined light curves exhibit a gradual brightening over the ~ 5000 d observation timescale (Figure 42a).

4 VARIATION OF OUTBURST AMPLITUDE

In addition to the regular orbital modulation, we have also seen variations in the amplitude of this modulation throughout associated long-term cycles of variability. Similar behaviour has already been reported in BeX sources such as A0588-66 (McGowan & Charles 2003) and SXP755 (Schmidtke et al. 2004). It has been suggested that the strength of the outbursts may depend on the density and extent of the equatorial disc at the time of periastron passage (see McGowan & Charles 2003; Schmidtke et al. 2004).

For the sources considered here, we investigate this relationship through figure 43 which plots the orbital outburst amplitude against the source brightness (presumed related to the size of the Be circumstellar disc). When the disc is larger (hence brighter), the neutron star’s eccentric orbit leads to a more significant interaction (and hence out-

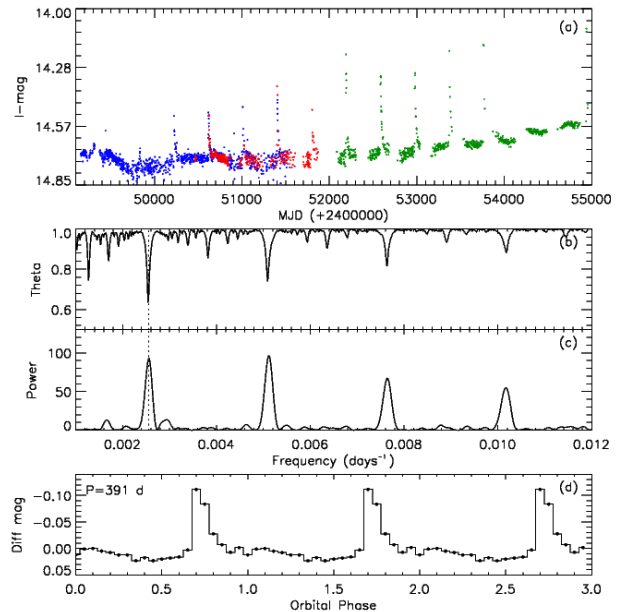


Figure 42. SXP755. (a): MACHO \mathcal{R} -band (blue), OGLE II (red) and OGLE III (green) light curves. (b) and (c): Power spectrum (PDM and LS) of the combined light curves showing a significant peak at 391 d and harmonics. (d): data folded on the 391 d period.

burst) during periastron passage. Conversely, when smaller, the disc interaction is weaker or absent completely.

Most of the SMC BeX sources exhibit an increase of outburst amplitude with brightness. The only exception is SXP7.92, which shows a decrease in strength of the outbursts when the source brightens. We suggest an explanation for this behaviour in section 5.1.

5 GENERAL DISCUSSION.

In this paper we have exploited the ~ 16 yr timebase of the MACHO and OGLE archives in order to investigate the long-term variability properties of almost all Be/X-ray pulsars currently known in the SMC. Virtually all of them show superorbital variations on timescales of hundreds to thousands of days. While such variations had been known historically for some of the bright, galactic Be systems, this is the first systematic study on these timescales of the BeX SMC population, and it is clear that such variability is extremely common, much of it appearing quasi-periodic in nature.

Optical light curves of these BeX systems show a variety of periodicities from as short as \sim hours (likely non-radial pulsation of the Be star) to tens of days (likely orbital modulation resulting from the neutron star’s regular interaction with mass lost from the Be donor in its eccentric orbit) to many hundreds of days, which we presume to be a property of the circumstellar disc surrounding the Be donor. This latter timescale is seen as both a low and high amplitude modulation, explanations for which range from an oscillation within the disc, to its formation and depletion. We will discuss these properties in more detail.

The list of all superorbital and orbital periods found in this report as well as the previously reported X-ray and optical periods are combined in table 3.

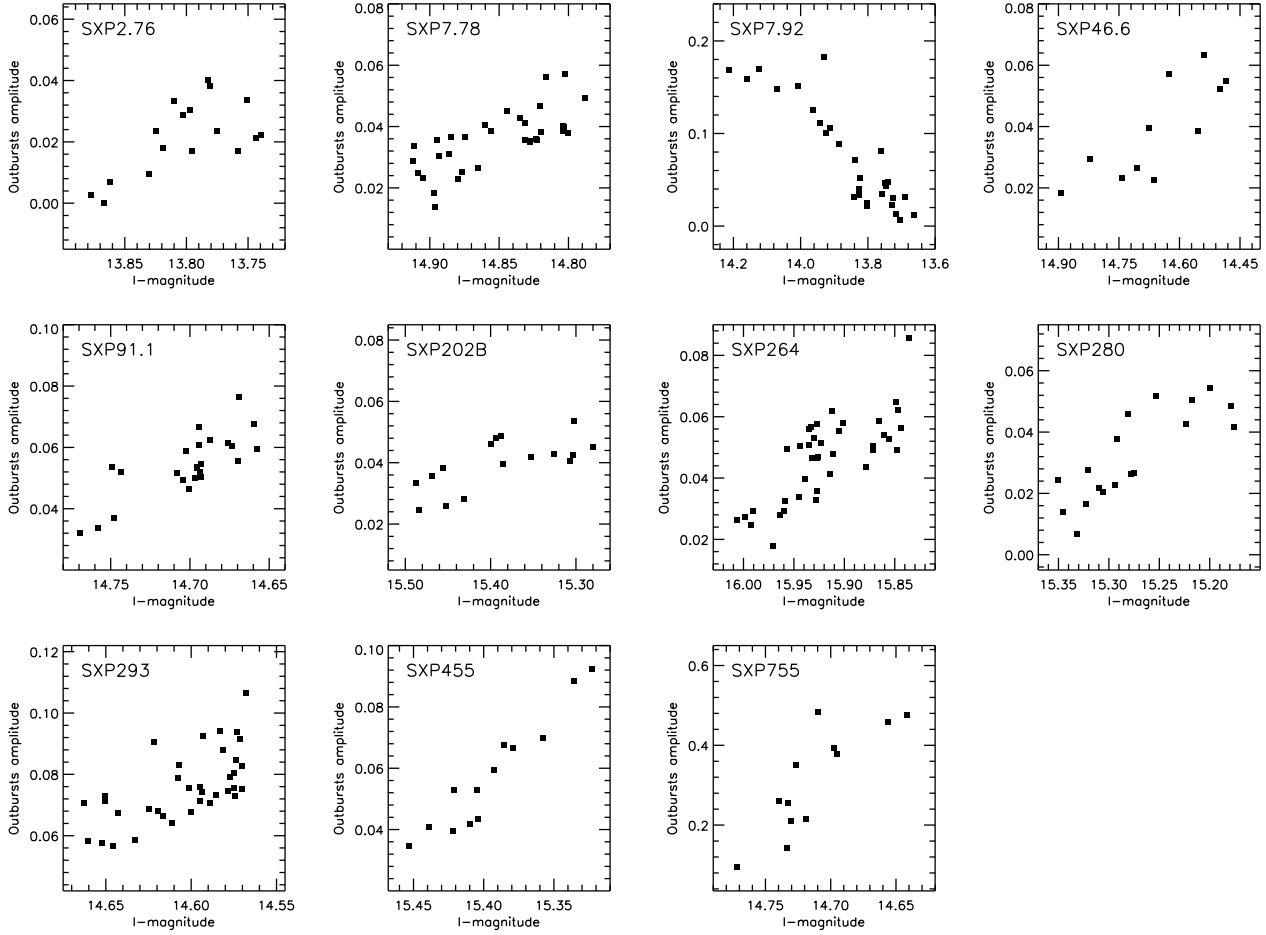


Figure 43. Variation of outburst amplitude of selected SMC BeX sources as a function of the brightness of the sources.

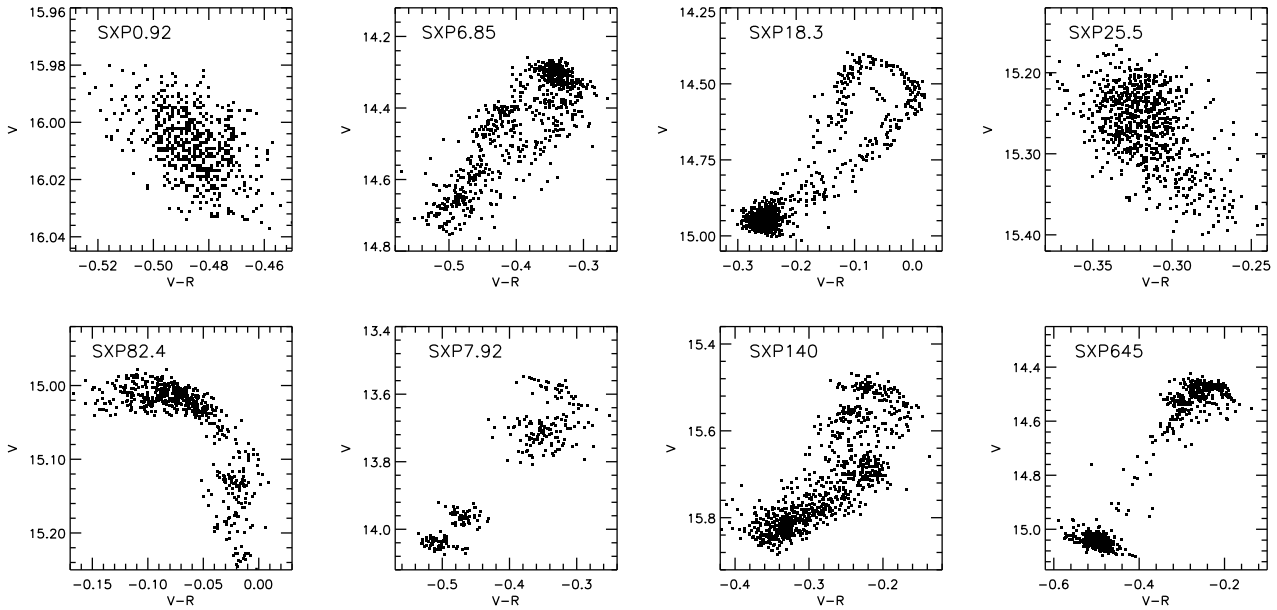


Figure 44. V vs. $V-R$ diagram of selected SMC BeX sources showing that they are redder when brighter; the 3 exceptions being SXP0.92, SXP25.5, and SXP82.4 which are redder when fainter.

5.1 Superorbital periods in BeX systems

Long-term non-orbital variations have previously been seen in some BeX systems, such as the 421 d quasi-periodic modulation in A0538-66 (Alcock et al. 2001). This modulation was the driving force behind the current paper, as it suggested as an observable effect of variations in size of the circumstellar disc around the Be star. Alcock et al. (2001) reported the additional remarkable property that, in A0538-66, the strength of the 16.5 d orbital outbursts depend very strongly on the brightness of the source and hence are also a function of the 421 d cycle. They occur during optical minimum, but not when the star is at its maximum brightness. For this system, the decline in brightness has been suggested to be related to the formation of an extended, cool, equatorial disc about the Be star, which will mask part of the Be star itself. A0538-66 becomes redder at minimum and bluer at optical maximum, which is what might be expected for a high inclination system. In contrast, we find here that only a few of the SMC BeX sources exhibit this type of behaviour, such as SXP25.5 (see figure 44).

However, for almost all of the SMC sources examined here, the source gets *redder* when it brightens (figure 44). For these systems, we interpret the red continuum as arising from the Be circumstellar disc seen at moderate or low inclination, i.e. the disc adds cooler light to that of the B star. BeX systems can exhibit this type of behaviour if the inclination of the Be equatorial disc is $\leq 90^\circ - \alpha$, where α is the opening angle of the disc (and is likely very small, \leq few degrees). Assuming that all the BeX binaries are oriented at random, the probability of a system having an inclination $i \leq 90^\circ - \alpha$ is simply $1 - \cos(90^\circ - \alpha)$. If we assume that the opening angle of the disc for a typical BeX source is $\alpha \sim 10^\circ$, then the probability of a BeX having an inclination $< 80^\circ$ is 0.83. i.e. we would therefore expect the BeX systems to exhibit this type of behaviour rather than that of A0538-66. In our sample of 31 sources with MACHO counterparts we would then expect only 4 or 5 sources to exhibit the ‘‘A0538-type’’ of behaviour, and this is consistent with the number (3 sources) that become redder as they get fainter (see figure 44).

In addition, we have seen a correlation between the amplitude of outburst and brightness in some sources (such as SXP7.78, SXP293, SXP755, ...). For those systems, the amplitude of outburst varies as a function of the brightness of the source, the amplitude growing with the source brightness (see figure 43). This suggests that the size of the Be equatorial disc influences the scale of the interaction between the neutron star and the Be equatorial disk.

However, if the Be equatorial disc becomes sufficiently large, then it can influence the entire orbit of the neutron star, producing a type II outburst. In this case, the Be circumstellar disk almost reaches its maximum size because it is then truncated by the neutron star. At this point the neutron star acts to increase the density of the disc rather than extend its size, hence the optical modulation is greatly reduced. This would explain the strange behaviour of SXP7.92. In Figure 44, the MACHO colour variation of SXP7.92 increases with the brightness of the source. However, its outburst amplitude becomes very weak as it brightens (Figure 43). For this system, the equatorial disc has be-

come very large (it increases in brightness by ~ 1 mag) and likely encompasses the entire orbit of the neutron star.

For highly variable sources (such as SXP6.85, SXP8.88, SXP15.3, SXP18.3,...), the MACHO colour variations follow the variation in brightness of the source. This confirms that the long-term variation in the light curve is related to the behaviour of the Be circumstellar disc.

5.1.1 Contribution of the extended disc.

Let us consider one of these highly variable SMC BeX sources. Assuming that SXP6.85 is viewed face-on ($i \sim 0^\circ$) and it has no disc during optical minimum, then the 0.7 mag global change in the light curve represents the brightness contribution from the Be disc. This implies a disc luminosity of $\sim 3.3 \times 10^{35} \text{ erg.s}^{-1}$, which corresponds to a total increase in brightness by $\sim 95\%$ from the optical minimum ($L_{\min} \sim 3.5 \times 10^{35} \text{ erg.s}^{-1}$). However, for a very high inclination system such as A0538-66 ($i \geq 74^\circ.9 \pm 6^\circ.5$, McGowan & Charles 2003), the quiescent state (no disc, only the naked B star) corresponds to the maximum optical brightness, and then when the equatorial disc grows it masks part of the Be star and reduces its optical brightness. The change in brightness in the light curve of A0538-66 is about 0.5 mag. However, the size of the equatorial disc of this source cannot be large because of its short orbital period ($P_{\text{orb}} = 16.65$ d, McGowan & Charles 2003), as the disc will be truncated at a smaller radius. The change in luminosity between no disc and maximum size of disc is about $2.7 \times 10^{35} \text{ erg.s}^{-1}$, this corresponds to a decrease in the total brightness of $\sim 37\%$ from its quiescent state.

5.1.2 Interaction with the neutron star.

It is interesting to note that, in spite of their long orbital periods, the presumed high orbital eccentricity leads to high neutron star velocities during periastron passage. Consider a typical BeX source consisting of a $1.4 M_\odot$ compact object orbiting a $10 M_\odot$ Be star with an eccentricity of $e = 0.7$ and orbital periods of $P_{\text{orb}} = 17$ d and 300 d. At periastron (separation = 1.3 and $8.9 \times 10^7 \text{ km}$), the neutron star would have a velocity of 443 and 170 km.s^{-1} respectively. The projected equatorial rotational velocity of a Be star ($v \sin i$) can be estimated from the broadening of its spectral lines, with a mean value of about 250 km.s^{-1} (Slettebak 1982), which is comparable to the neutron star velocity at periastron. Therefore, at periastron, the primary star is rotating close to corotation with the orbiting neutron star.

5.1.3 One-armed oscillation in the equatorial disc.

Be stars are believed to exhibit a cyclic variation in their emission line profiles (known as the ‘V/R’ variations; McLaughlin 1961). It is widely accepted that these variations are caused by global one-armed oscillations in the equatorial discs of Be stars (Kato 1983; Okazaki 1991). The period of this long-term V/R variation is typically in the range of 2-15 years for isolated Be stars (eg. Papaloizou, Savonije, & Henrichs 1992). We note that these timescales are very similar to those seen in our light curves (see Table 3). This suggests that the long-term variation

in Be star emission line profiles (the ‘V/R’ variation) may be related to the long-term variations we see in the optical light curves. Unfortunately, there are not yet any long-term spectroscopic studies of these SMC BeX sources capable of investigating the correlation between these two (photometric and spectroscopic) long-term variations.

The peaks and dips seen in SXP2.37 may possibly be explained as a direct effect of such a precessing elongated disk. For SXP2.37, the outbursts are seen during optical maximum, and then change into dips as the source fades. If we assume that SXP2.37 is a high inclination system, the source is brighter when the elongated disc extends to each side of the Be star, in this case the interaction between the neutron star and the disc can be seen as a maximum. On the other hand, when the elongated disc passes in front it will obscure the Be star, reducing its brightness. In this case, the neutron star passage will enlarge the disc which blocks some light from the hotter Be star, which we see as dips.

5.2 Orbital and Super-orbital period correlation

Apart from the very long-term (~ hundreds of days) variations that are of primary interest here, we have also seen optical orbital modulations in the light curves of these SMC BeX systems, visible as a series of regular outbursts. These outbursts are interpreted as the periastron passage of the neutron star where it interacts with the Be equatorial disc. At periastron, the circumstellar disc can be perturbed from its stable resonant state, this perturbation will slightly increase its surface area and, hence, its optical brightness (Okazaki & Negueruela 2001).

The optical light curves folded on the orbital period have an asymmetric profile, with a faster rise and slower decline. This behaviour has been seen in other BeX systems (Alcock et al. 2001). Furthermore, in some sources such as SXP46.6, SXP327, SXP348, etc., the optical outburst is not just a single maximum, but can show two peaks every binary cycle, which is seen in the light curves when folded on the orbital period. McGowan et al. (2007), and Coe et al. (2009) suggested this behaviour as arising from the misalignment between the spin axis of the Be equatorial disc and the orbital plane of the binary system. Therefore, the neutron star interacts twice with the Be equatorial disc every binary cycle. We note that for SXP18.3, we find an optical periodicity (P= 28.5 d) that is distinct from its presumed orbital period (P= 17.92 d), which is clearly seen only in the MACHO, OGLE II, and first year of the OGLE III light curves. The mechanism that produces this 28.5 d optical modulation is not understood but it is clearly visible in the light curve. We note that it appears especially during the optical minimum.

The observed misalignment can be caused by the supernova kick received by the system when the neutron star was born. Brandt & Podsiadlowski (1995) suggested that an asymmetric supernova explosion can give very large kicks to the newly formed neutron stars which can either disrupt the system if the kick is too strong or lead to a large eccentricity and misalignment between the old and new orbits if the velocity of the kick is smaller. Martin, Tout, & Pringle (2009) suggested that a velocity kick of 265 km.s⁻¹ is consistent with the observed misalignments in BeX systems, but too high for the observed eccentricities.

In Figure 45, we have plotted the observed long-term

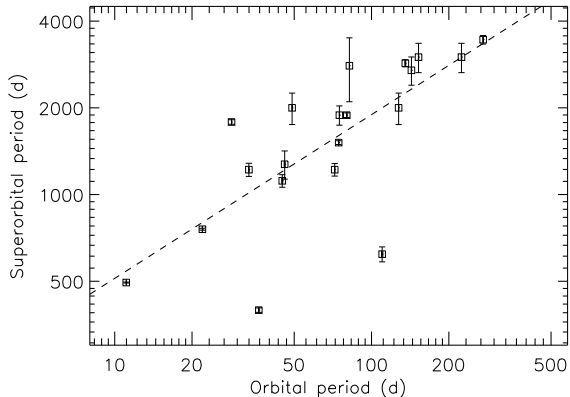


Figure 45. Plot of the BeX superorbital periods found in this work against orbital period. The dashed line represents the best linear fit.

superorbital period of the SMC BeX systems against their orbital periods. It appears that the two periods correlate. We have computed the linear Pearson correlation coefficient to be 0.73 with a p-value of 0.00039 (significant at the 99.9% confidence level). Some authors have already suggested that these long-term variations might be related to the orbital period (Reig et al. 2005; Coe et al. 2005), based on the H α EW - P_{orb} relationship of Reig, Fabregat, & Coe (1997), which is in good agreement with the disc truncation model of Okazaki & Negueruela (2001). If the Be equatorial disc is truncated by the neutron star orbit, a source with a shorter period (large number of periastron passages) would have a smaller equatorial disc than a source with a wider and more eccentric orbit.

6 SUMMARY

In summary, we have studied the long-term properties of SMC Be X-ray binaries. We have found 19 superorbital periods which we suggest are related to properties of the Be circumstellar disc (see table 3). In addition, we have compiled and updated the orbital periods of these BeX sources using the complete MACHO, OGLE II, and OGLE III databases.

Furthermore, the amplitude of these outbursts vary significantly through the superorbital cycle. They are very strong either at optical maxima or at optical minima, depending on the inclination of the source. For high inclination systems, the Be circumstellar disc will mask the hotter and bluer star, and their outburst amplitudes will be strong at optical minima.

ACKNOWLEDGMENTS

We are grateful to Luis Balona, Malcom Coe, Brian Warner, Matthew Schurch, Lee Townsend, Brian Van Soelen and Patricia Whitelock for useful discussions. We also thank the anonymous referee for useful suggestions, particularly in clarifying the significance or otherwise of the low amplitude modulation. AFR is supported financially by the South African SKA project.

Table 3. Periodicities found in SMC BeX sources.

Short	P_{sup}^*		P_{orb}		Previously reported	
ID	Period [d]	Semi – amplitude [mmag]	Period(error) [d]	Semi – amplitude [mmag]	$P_{\text{X-ray}}^\dagger$ [d]	P_{opt} [ref] [d]
SXP0.09	[247]	<5	...	<5
SXP0.92	2654±298	6	...	<5	...	51[1]
SXP2.37	...	<5	18.58(1)**	16
SXP2.76	2800±700	73	82.37(7)	11	...	82.1[2]
SXP3.34	[495]	<5	11.09(1)	14
SXP6.85	621±4	201	110.0(2)	26	112	114[4]
SXP7.78	1116±56	50	44.9(2)	26	44.9	44.8[5]
SXP7.92	397±2	138	36.41(2)	15	...	36.8[14]
SXP8.9	1786±32	485	28.51(1)	8	28.4	33.4[6]
SXP9.13	1886±35	32	80.1(1)	8	77.2	40.1[8]
SXP15.3	1515±23	55	74.51(5)	12	28	75.1[8]
SXP18.3	...	<5	17.95(1)	12	17.7	17.7[15]
SXP22.1	...	<5	75.97(6)	9
SXP25.5	...	<5	22.50(1)	16
SXP31.0	...	<5	90.5(1)	14	...	90.4[2]
SXP34.1	...	<5	[598]	<5
SXP46.6	...	<5	136.4(2)	9	137	137[9]
SXP59	...	<5	62.10(4)	8	122	60.2[10]
SXP74.7	1220±64	21	33.37(1)	12	61.6	33.4[11]
SXP82.4	...	<5	171(1)	10	362	...
SXP91.1	...	<5	88.3(1)	24	117	88.2[7]
SXP101	758±6	14	21.95(1)	12	25.2	21.9[12]
SXP138	2700±304	172	[143.1]	<5	103	122[6]
SXP140	492±2.4	110	...	<5	...	197[6]
SXP172	...	<5	67.88(4)	22	70	69.9[6]
SXP202A	1220±61	100	71.98(5)	18	91	...
SXP202B	~3000	108	224(1)	15
SXP264	~2000	47	49.06(2)	18	...	49.1[10]
SXP280	~2000	88	126.4(2)	15	64.8	127[2]
SXP293	...	<5	59.77(3)	35	151	59.7[7]
SXP304	...	<5	[344]	<5	...	520[6]
SXP327	1274±143	41	45.9(2)	120	...	45.9[16]
SXP348	...	<5	94.4(1)	9	...	93.9[6]
SXP455	1886±145	110	74.96(5)	21	...	74.7[7]
SXP504	3448±119	32	272(1)	10	265	273[10]
SXP564	~3000	69	152.4(2)	15	151	95.3[7]
SXP645	2857±81	460	[135.3]	<5
SXP701	...	<5	412(5)	8	...	412[10]
SXP755	...	<5	391(2)	66	389	394[7]

[1]: Kaspi et al. (1993); [2]: Schmidtke & Cowley (2006); [3]: Coe et al. (2005); [4]: McGowan et al. (2008); [5]: Cowley & Schmidtke (2004); [6]: Schmidtke, Cowley, & Udalski (2006); [7]: Schmidtke et al. (2004); [8]: Edge (2005a); [9]: McGowan et al. (2008); [10]: Schmidtke & Cowley (2005b); [11]: Schmidtke & Cowley (2007b); [12]: McGowan et al. (2007); [13]: Edge et al. (2005b); [14]: Coe et al. (2009); [15]: Schurch et al. (2009); [16]: Udalski & Coe (2008)

Periods in square brackets are marginally significant (see section 2.3).

** 1 σ uncertainty in parentheses (units of last digit).

*Superorbital period.

\dagger X-ray orbital period from Galache et al. (2008).

This paper utilizes public domain data obtained by the MACHO Project, jointly funded by the US Department of Energy through the University of California, Lawrence Livermore National Laboratory under contract No. W-7405-Eng-48, by the National Science Foundation through the Center for Particle Astrophysics of the University of California under cooperative agreement AST-8809616, and by the Mount Stromlo and Siding Spring Observatory, part of the Australian National University. The OGLE project is partially supported by the Polish MNiSW grant N20303032/4275.

REFERENCES

- Ables J. G., Jacka C. E., Hall P. J., Hamilton P. A., McConnell D., McCulloch P. M., 1987, IAUC, 4422, 1
 Alcock C., et al., 1996, MNRAS, 280, L49
 Alcock C., et al., 2001, MNRAS, 321, 678
 Allen D., 1977, IAUC, 3143, 1
 Bell J. F., 1994, PASAu, 11, 81
 Brandt N., Podsiadlowski P., 1995, MNRAS, 274, 461
 Buckley D. A. H., Coe M. J., Stevens J. B., van der Heyden K., Angelini L., White N., Giommi P., 2001, MNRAS, 320, 281
 Chakrabarty D., Levine A. M., Clark G. W., Takeshima T., 1998, IAUC, 7048, 1
 Charles P. A., Southwell K. A., O’Donoghue D., 1996,

- IAUC, 6305, 2
 Clark G., Remillard R., Woo J., 1996, IAUC, 6282, 1
 Coe M. J., Edge W. R. T., Galache J. L., McBride V. A., 2005, MNRAS, 356, 502
 Coe M. J., Gaensicke B. T., 2003, ATel, 123, 1
 Coe M. J., Haigh N. J., Reig P., 2000, MNRAS, 314, 290
 Coe M. J., Schurch M., McBride V. A., Corbet R. H. D., Townsend L. J., Udalski A., Galache J. L., 2009, MNRAS, 394, 2191
 Coe M. J., Stevens J. B., Buckley D. A. H., Charles P. A., Southwell K. A., 1998, MNRAS, 293, 43
 Corbet R., Markwardt C. B., Marshall F. E., Laycock S., Coe M., 2002, IAUC, 7932, 2
 Corbet R., Marshall F. E., Lochner J. C., Ozaki M., Ueda Y., 1998, IAUC, 6803, 1
 Corbet R. H. D., 1986, MNRAS, 220, 1047
 Corbet R. H. D., 1984, A&A, 141, 91
 Corbet R. H. D., Coe M. J., Edge W. R. T., Laycock S., Markwardt C. B., Marshall F. E., 2004a, ATel, 277, 1
 Corbet R. H. D., Coe M. J., Marshall F. E., McBride V. A., Schurch M. P. E., 2008, ATel, 1600, 1
 Corbet R. H. D., Markwardt C. B., Coe M. J., Edge W. R. T., Laycock S., Marshall F. E., 2004b, ATel, 273, 1
 Corbet R. H. D., Markwardt C. B., Coe M. J., Edge W. R. T., Laycock S., Marshall F. E., 2003b, ATel, 214, 1
 Corbet R. H. D., Markwardt C. B., Marshall F. E., Coe M. J., Edge W. R. T., Laycock S., 2003a, ATel, 163, 1
 Covino S., Negueruela I., Campana S., Israel G. L., Polcaro V. F., Stella L., Verrecchia F., 2001, A&A, 374, 1009
 Cowley A. P., Schmidtke P. C., 2004, AJ, 128, 709
 Cowley A. P., Schmidtke P. C., McGrath T. K., Ponder A. L., Fertig M. R., Hutchings J. B., Crampton D., 1997, PASP, 109, 21
 Edge W. R. T., Coe M. J., 2003a, MNRAS, 338, 428
 Edge W. R. T., Coe M. J., Corbet R. H. D., Markwardt C. B., Laycock S., Marshall F. E., 2003b, ATel, 215, 1
 Edge W. R. T., et al., 2005b, MNRAS, 361, 743
 Edge W. R. T., Coe M. J., McBride V. A., 2004, ATel, 217, 1
 Edge W. R. T., 2005a, PhDT,
 Eger P., Haberl F., 2008, ATel, 1453, 1
 Galache J. L., Corbet R. H. D., Coe M. J., Laycock S., Schurch M. P. E., Markwardt C., Marshall F. E., Lochner J., 2008, ApJS, 177, 189
 Haberl F., Eger P., Pietsch W., 2008a, A&A, 489, 327
 Haberl F., Eger P., Pietsch W., Corbet R. H. D., Sasaki M., 2008b, A&A, 485, 177
 Haberl F., Pietsch W., 2004, A&A, 414, 667
 Haberl F., Pietsch W., Kahabka P., 2007, ATel, 1095, 1
 Haberl F., Pietsch W., Schartel N., Rodriguez P., Corbet R. H. D., 2004, ATel, 219, 1
 Haberl F., Sasaki M., 2000, A&A, 359, 573
 Hughes J. P., 1994, ApJ, 427, L25
 Hughes J. P., Smith R. C., 1994, AJ, 107, 1363
 Imanishi K., Yokogawa J., Koyama K., 1998, IAUC, 7040, 2
 Israel G. L., Stella L., Angelini L., White N. E., Giommi P., Covino S., 1997, ApJ, 484, L141
 Israel G. L., Stella L., Campana S., Covino S., Ricci D., Oosterbroek T., 1998, IAUC, 6999, 1
 Israel G. L., Stella L., Covino S., Campana S., Mereghetti S., 1999, IAUC, 7101, 1
 Kaspi V. M., Johnston S., Manchester R. N., Bailes M., Bell J. F., Bessell M., Lyne A. G., D'Amico N., 1993, BAAS, 25, 1434
 Kato S., 1983, PASJ, 35, 249
 Lamb R. C., Macomb D. J., Prince T. A., Majid W. A., 2002, ApJ, 567, L129
 Lamb R. C., Prince T. A., Macomb D. J., Finger M. H., 1999, IAUC, 7081, 4
 Laycock S., Corbet R. H. D., Coe M. J., Marshall F. E., Markwardt C., Edge W., 2003, MNRAS, 339, 435
 Laycock S., Corbet R. H. D., Coe M. J., Marshall F. E., Markwardt C., Lochner J., 2005, ApJS, 161, 96
 Laycock S., Zezas A., Hong J., 2008, arXiv, arXiv:0809.1738
 Leong C., Kellogg E., Gursky H., Tananbaum H., Giacconi R., 1971, ApJ, 170, L67
 Li F., Jernigan G., Clark G., 1977, IAUC, 3125, 1
 Lomb N. R., 1976, Ap&SS, 39, 447
 Lucke R., Yentis D., Friedman H., Fritz G., Shulman S., 1976, ApJ, 206, L25
 Macomb D. J., Finger M. H., Harmon B. A., Lamb R. C., Prince T. A., 1999, ApJ, 518, L99
 Macomb D. J., Fox D. W., Lamb R. C., Prince T. A., 2003, ApJ, 584, L79
 Majid W. A., Lamb R. C., Macomb D. J., 2004, ApJ, 609, 133
 Marshall F. E., et al., 1998, IAUC, 6818, 1
 Marshall F. E., Lochner J. C., Takeshima T., 1997, IAUC, 6777, 2
 Martin R. G., Tout C. A., Pringle J. E., 2009, MNRAS, 397, 1563
 McGowan K. E., Charles P. A., 2003, MNRAS, 339, 748
 McGowan K. E., et al., 2007, MNRAS, 376, 759
 McGowan K. E., Coe M. J., Schurch M. P. E., Corbet R. H. D., Galache J. L., Udalski A., 2008, MNRAS, 384, 821
 McLaughlin D. B., 1961, JRASC, 55, 73
 Meyssonier N., Azzopardi M., 1993, A&AS, 102, 451
 Negueruela I., 1998, A&A, 338, 505
 Okazaki A. T., Negueruela I., 2001, A&A, 377, 161
 Okazaki A. T., 1991, PASJ, 43, 75
 Papaloizou J. C., Savonije G. J., Henrichs H. F., 1992, A&A, 265, L45
 Pesch P., Sanduleak N., Philip A. G. D., 1977, IAUC, 3127, 3
 Reig P., Fabregat J., Coe M. J., 1997, A&A, 322, 193
 Reig P., Negueruela I., Fabregat J., Chato R., Coe M. J., 2005, A&A, 440, 1079
 Roberts D. H., Lehar J., Dreher J. W., 1987, AJ, 93, 968
 Sasaki M., Haberl F., Keller S., Pietsch W., 2001, A&A, 369, L29
 Sasaki M., Pietsch W., Haberl F., 2003, A&A, 403, 901
 Scargle J. D., 1982, ApJ, 263, 835
 Schmidtke P. C., Cowley A. P., 2007a, ATel, 1181, 1
 Schmidtke P. C., Cowley A. P., 2006, AJ, 132, 919
 Schmidtke P. C., Cowley A. P., 2005b, AJ, 130, 2220
 Schmidtke P. C., Cowley A. P., Crane J. D., Taylor V. A., McGrath T. K., Hutchings J. B., Crampton D., 1999, AJ, 117, 927
 Schmidtke P. C., Cowley A. P., Levenson L., Sweet K., 2004, AJ, 127, 3388
 Schmidtke P. C., Cowley A. P., Udalski A., 2009, ATel,

- 1992, 1
 Schmidtke P. C., Cowley A. P., Udalski A., 2006, AJ, 132, 971
 Schmidtke P. C., Cowley A. P., 2007b, AAS, 38, 724
 Schmidtke P. C., Cowley A. P., 2005a, ATel, 648, 1
 Schulz, M. 2002, Computers and Geosciences, 28, 421
 Schurch M., Udalski A., Coe M., 2008, ATel, 1670, 1
 Schurch M. P. E., et al., 2009, MNRAS, 392, 361
 Slettebak A., 1982, ApJS, 50, 55
 Stellingwerf R. F., 1978, ApJ, 224, 953
 Stevens J. B., Coe M. J., Buckley D. A. H., 1999, MNRAS, 309, 421
 Udalski A., 2008, AcA, 58, 187
 Udalski A., Szymanski M. K., Soszynski I., Poleski R., 2008, AcA, 58, 69
 Udalski A., Coe M. J., 2008, ATel, 1458, 1
 Udalski A., Kubiak M., Szymanski M., 1997, AcA, 47, 319
 Ueno M., Yokogawa J., Imanishi K., Koyama K., Torii K., Kohmura T., 2001, ASPC, 251, 420
 Ueno M., Yamaguchi H., Takagi S.-I., Yokogawa J., Koyama K., 2004, PASJ, 56, 175
 Webster B. L., Martin W. L., Feast M. W., Andrews P. J., 1972, Natur, 240, 183
 Yokogawa J., Koyama K., 2000, IAUC, 7361, 2
 Yokogawa J., Koyama K., 1998b, IAUC, 7009, 3
 Yokogawa J., Koyama K., 1998d, IAUC, 6835, 2
 Yokogawa J., Koyama K., 1998a, IAUC, 6853, 2
 Yokogawa J., Imanishi K., Ueno M., Koyama K., 2000c, PASJ, 52, L73
 Yokogawa J., Torii K., Imanishi K., Koyama K., 2000b, PASJ, 52, L37
 Yokogawa J., Torii K., Kohmura T., Imanishi K., Koyama K., 2000a, PASJ, 52, L53
 Zaritsky D., Harris J., Thompson I. B., Grebel E. K., Massey P., 2002, AJ, 123, 855
 Zebrun K., et al., 2001, AcA, 51, 317